

# MIMO Applications for Multibeam Satellites

Robert T. Schwarz, *Member, IEEE*, Thomas Delamotte, *Member, IEEE*,  
Kai-Uwe Storek, *Member, IEEE*, and Andreas Knopp, *Senior Member, IEEE*

**Abstract**—High throughput satellites employing multi-beam antennas and full frequency reuse for broadband satellite services are considered in this paper. Such architectures offer, for example, a cost-effective solution to optimize data delivery and extend the coverage areas in future 5G networks. We propose the application of the multiple-input-multiple-output (MIMO) technology in both the feeder link and the multiuser downlink. Spatial multiplexing of different data streams is performed in a common feeder beam. In the user links, MIMO with multiple beams is exploited to simultaneously serve different users in the same frequency channel. Under particular design constraints, effective spatial separation of the multiple user signals is possible. To mitigate the inter-stream interference in the MIMO feeder link as well as the multiuser downlink, precoding of the transmit signals is applied. Simulation results illustrate the performance gains in terms of sum throughput.

**Index Terms**—MIMO, satellite communication, channel capacity, multiuser channels, radiowave propagation, 5G, precoding, user scheduling, non-terrestrial networks, backhauling, access networks

## I. INTRODUCTION

Broadcasting of video content to home users has been the key application scenario of geostationary satellite systems for many decades. Meanwhile, the advent of 5G networks and the introduction of integrated satellite-terrestrial architectures will considerably change the role of satellite communications in the near future. Traffic offloading to the network edges, backhauling or direct broadband access (e.g., Video-on-Demand) to remote areas belong to the most promising use cases of satellite communications (SATCOM) [1]. Other use cases include the delivery of broadband data to satellite earth stations on mobile platforms (ESOMPs) like trains, cruise ships and airplanes. The cost-per-bit is in this context a key enabler. The sustaining

demand for higher data rates in next-generation networks has already motivated the development of high throughput satellites (HTSs).

To meet the target data rates of future HTS systems and the economies of scale in terms of costs per bit as required by 5G applications and networks, the trend has been to increase the number of beams to provide higher power flux density per beam and increase the reuse factors for the spectrum. In contrast to a four color frequency reuse (FR4) scheme, where orthogonality between the adjacent beams is ensured using disjoint frequencies and polarizations, the full frequency reuse (FFR) of the spectrum has recently been considered [2]. However, FFR leads to significant inter-beam interference, also called co-channel interference (CCI), and moves the power-limited link budget to an interference-limited regime. Users located at the edges of the beams suffer from the most severe CCI and experience a strong degradation of their achievable carrier to interference plus noise power ratio (CINR).

One strategy to significantly reduce the CCI is the precoding of the transmit signals in the gateways. In general, linear and nonlinear precoding techniques can be considered. While nonlinear precoders are hard to implement in practical systems, thus serving only as a theoretical upper limit in many studies, linear precoding techniques often achieve similar performances like their nonlinear counterparts [3]. Remarkable throughput improvements compared to the widespread FR4 scheme can be achieved with linear precoding strategies like for example zero-forcing (ZF) [4]. Recent research activities in [5] and [6] have a special focus on precoding for multicast communication to exploit potential throughput gains offered by the DVB-S2X superframes [7].

To support the huge amount of aggregated user traffic, the shift of the feeder links to the Q/V-band offering unexplored spectrum of up to 5 GHz in bandwidth has recently been considered [8]. Nevertheless, several gateways are still necessary [9]. The gateways have to be displaced geographically

Manuscript submitted May 30, 2018; revised August 8, 2018, and October 18, 2018.

R. T. Schwarz, T. Delamotte, K.-U. Storek, and A. Knopp are with the Chair of Signal Processing, Bundeswehr University Munich, 85579 Neubiberg, Germany (e-mail: papers.sp@unibw.de).

to allow the reuse of the feeder link bandwidth. Moreover, transmit diversity techniques are needed to cope with the heavy rain fades in these frequency bands [10]. Different solutions can be found in the literature, e.g. in [11] and the references therein. All solutions are based on a certain amount of redundancy in the feeder links, either through additional gateways in standby that become active if one gateway is in outage, or through spare capacity which is reserved at the active gateways. For traffic re-routing, a terrestrial network to interconnect the gateways is presumed in all cases, which is already common practice in current systems.

Relying on the existing gateway infrastructures as well as resorting to the FFR strategy in the user beams, we propose the application of spatial multiple-input-multiple-output (MIMO) techniques to tackle the uplink and downlink bandwidth limitations and to reduce the per-bit delivery costs. MIMO systems are well-known for their bandwidth efficiency through the simultaneous transmission of multiple data streams in the same frequency band. This is among the most important performance indicators to compete with terrestrial Gigabit networks. Under favorable channel conditions, the spatial interference is eliminated in the channel, and a linear increase of the channel capacity with the number of transmit or receive antennas, whatever number is smaller, is achieved.

In MIMO channels with predominant line-of-sight (LOS) wave propagation, particular antenna array geometries are required [12] to obtain such favorable channel conditions. The optimal antenna array geometry for maximum-capacity LOS MIMO satellite channels has been analytically derived in [13] and was verified through satellite channel measurements reported in [14]–[16]. Based on these fundamentals, very recent research has now started to propose first practical applications of MIMO to SATCOM [17]. Here, the distribution of Video-on-Demand (VoD) services as an example of edge content delivery to home users in future 5G satellite networks is addressed [18]. However, the results can also be further extended to other fixed satellite service (FSS) applications like the ESOMPs.

In this paper we consider the forward link of a HTS system. In particular, we propose a MIMO feeder uplink with two gateway antennas and a multiuser MIMO (MU-MIMO) downlink to non-cooperative users with a single antenna each. The

satellite payload relies on a bent-pipe architecture [19, Chapter 9.2, p. 437] in order to keep the complexity at satellite level low. The content delivery to the users is achieved through spatial multiplexing of the different data streams.

The use of spatial MIMO in the uplink and in the downlink is a completely different approach compared to satellite network architectures that have been proposed so far. In state-of-the-art feeder links, the deployment of antennas separated by several tens of kilometers is only done to achieve diversity gains within the footprint of a given feeder beam. Both antennas are never active at the same time, which is not a cost-efficient solution due to the unused redundant hardware. With MIMO feeder links, the antennas are operated simultaneously, which doubles the maximum transmit power per link and enables spatial multiplexing. The opportunities of MIMO feeder links have been discussed by the authors in [20].

In the MU-MIMO downlink, the exploitation of the LOS channel phase information allows to build groups of users with limited CCI. These users are spread over an area covered by different beams and are scheduled within the same time slots. The proposed MIMO solution introduces a novel philosophy that does not try to arbitrarily allocate users to a predefined beam according to their position in the multibeam coverage as suggested in known schemes [2]. That way, in a MIMO FFR scheme, the beam pattern is resolved and reduced to nothing more than a shaping of the power flux density on Earth. Such a beamfree approach was first proposed in [17]. In a further step, this new concept might be used as another degree of freedom for throughput optimization, even leading to dynamically adaptable shaping depending on the capabilities of the satellite antenna multibeam architecture. In this work, an innovative HTS system design with a joint optimization of a smart gateway relying on spatial MIMO together with a novel scheduling algorithm in the user links is addressed.

In order to follow the proposed ideas for the novel MIMO HTS application, some basic findings on MIMO for LOS satellite channels are needed. Section II has been reserved for this aspect. The proposed MIMO HTS system is then thoroughly described in Section III, and the performance is assessed in terms of the sum throughput in Section IV. Section V concludes the paper.

**Notation:**  $\mathbf{I}_M$  denotes the  $M \times M$  identity matrix and  $\mathbf{1}$  is an all-ones vector of proper dimension. Operator  $(\cdot)^*$  denotes the complex conjugate while  $(\cdot)^T$  and  $(\cdot)^H$  denote the transpose and the complex conjugate transpose of a matrix or a vector. The functions  $\text{diag}\{\cdot\}$  and  $\text{tr}\{\cdot\}$  abbreviate the diagonal and trace operators. The notation  $\|\cdot\|$  represents the Euclidean vector norm and  $|\cdot|$  gives the absolute value of a scalar. The operator  $\min\{\cdot\}$  (or  $\max\{\cdot\}$ ) returns the minimum (or maximum) value. The symbol  $\odot$  is the Hadamard product, i.e. the element-wise multiplication of two matrices, and the operator  $\lfloor x \rfloor$  gives the greatest integer less than or equal to  $x$ . Finally,  $(\cdot)^+$  represents the Moore-Penrose pseudo-inverse of a matrix.

## II. MIMO SATCOM BASICS

In this section, the basics on MIMO over satellite for FSS are summarized. The focus is on the MIMO satellite channel and its correct modeling as a prerequisite for reliable system performance predictions. The channel capacity is used as a measure to assess the channel properties. We will show that the signal phase is a key property of the electromagnetic (EM) waves that needs to be considered in order to obtain high MIMO gains. We introduce the MIMO free space propagation model and neglect atmospheric effects for now. However, Section II-F will later be solely devoted to the discussion of atmospheric effects. Since the free space medium is isotropic, the channel is reciprocal and it is, therefore, sufficient to initially concentrate on the downlink. The presented results provide the necessary fundamentals for the discussion of the proposed MIMO HTS system architecture covering both the uplink and the downlink channel.

### A. Free Space MIMO SATCOM Channel Model

We consider a MIMO satellite downlink for FSS between  $N$  satellite transmit antennas in the geostationary earth orbit (GEO) and  $M$  earth station receive antennas. The satellite acts as the MIMO transmitter while the fixed earth station is the MIMO receiver. The vector  $\mathbf{y} = [y_1, \dots, y_M]^T$  is the vector of receive signals at a given time instance with  $y_m$  denoting the signal in complex baseband notation at the  $m$ -th receive antenna.  $\mathbf{y}$  is calculated as

$$\mathbf{y} = \mathbf{H}\mathbf{x} + \boldsymbol{\eta}, \quad (1)$$

with  $\mathbf{x} = [x_1, \dots, x_N]^T$  and  $\boldsymbol{\eta} = [\eta_1, \dots, \eta_M]^T$ . The symbols  $x_n$  and  $\eta_m$  are the transmit symbol at the  $n$ -th satellite antenna and the noise contribution at the  $m$ -th receive antenna, respectively. The noise entries are independent and identically distributed (i.i.d.) circularly symmetric complex Gaussian variables which are uncorrelated with the data symbols. The matrix  $\mathbf{H} \in \mathbb{C}^{M \times N}$  denotes the MIMO channel matrix. The calculation of its entries is detailed in the following.

We focus on frequency bands well above 10 GHz. In those frequency bands, high-gain and directive antennas are required to obtain a sufficient link budget and close the link with high throughput. Moreover, narrow main beams with low side lobe levels effectively suppress interfering signals from and to neighboring satellite systems, and are, therefore, a design objective for earth station antennas operating with GEO satellites [21]. Relying on such typical earth station antennas, it is assumed that any multipath contributions are suppressed by the directional antennas. Neglecting the atmospheric effects, the satellite channel can be described using a deterministic LOS model based on the free space wave propagation.

The LOS channel coefficient  $h_{mn}$  between the  $n$ -th satellite antenna and the  $m$ -th earth station antenna, which corresponds to the  $(m, n)$ -th entry of  $\mathbf{H}$ , is given in the equivalent baseband notation by

$$h_{mn} = a_{mn} \cdot e^{-j\frac{2\pi}{\lambda_c} r_{mn}} \approx a \cdot e^{-j\frac{2\pi}{\lambda_c} r_{mn}}. \quad (2)$$

Here,  $\lambda_c = c_0/f_c$  denotes the wavelength of the carrier with frequency  $f_c$ ,  $c_0$  is the speed of light, and  $a_{mn} = \lambda_c/(4\pi r_{mn}) \cdot e^{j\varphi}$  models the free space propagation gain. The parameter  $\varphi$  stands for the common carrier phase and can be assumed to be zero without loss of generality (w.l.o.g.). The parameter  $r_{mn}$  denotes the distance between the  $n$ -th satellite transmit antenna and the  $m$ -th earth station receive antenna. On the right hand side of (2), we applied the approximation  $a_{mn} \approx a = \lambda_c/(4\pi\bar{r})$  with  $\bar{r} = 1/(MN) \cdot \sum_{m=1}^M \sum_{n=1}^N r_{mn}$ . This is reasonable because the difference between the path lengths is very

small compared to their mean total length.<sup>1</sup> Note again that this model will be extended in subsection II-F to additionally take relevant atmospheric effects into account.

It is also important to note that ray tracing through the parameter  $r_{mn}$  has been applied to exactly determine the phase entries of  $\mathbf{H}$ . This is referred as the spherical wave model (SWM) in the literature and stands in contrast to the plane wave model (PWM) which assumes no relevant phase differences between the entries of  $\mathbf{H}$  [22]. As shown in the following, the application of the SWM is a fundamental prerequisite to correctly forecast the capacity provided by a MIMO satellite system and to derive the relevant design criteria for its capacity optimization. This is detailed in the next section.

### B. MIMO Channel Capacity

Consider again the downlink scenario, in which the single-satellite is the MIMO transmitter and the earth station is the MIMO receiver. Based on the deterministic LOS model in (2), the time invariant MIMO channel capacity without channel knowledge at the transmitter is given by [23]

$$C = \log_2 \left( \det \left( \mathbf{I}_M + \rho \cdot \mathbf{H}\mathbf{H}^H \right) \right). \quad (3)$$

Here,  $\rho$  is the carrier to noise power ratio (CNR), which is defined as the ratio of the transmit power per satellite antenna to the noise power per earth station receive antenna.

To illustrate the dependence of the channel capacity on the properties of  $\mathbf{H}$ , let us decompose the MIMO channel into parallel sub-channels, so called eigenmodes, with a singular value decomposition (SVD) of the form  $\mathbf{H} = \mathbf{U}\mathbf{V}\mathbf{H}$ . Moreover, to ease the mathematical notation,  $V = \max \{M, N\}$  and  $U = \min \{M, N\}$  are introduced. The matrices  $\mathbf{U}$  and  $\mathbf{V}$  are both unitary and constitute an orthonormal basis of the column and row spaces of the channel matrix  $\mathbf{H}$ , respectively. The matrix  $\mathbf{\Gamma}$  is a rectangular diagonal matrix with  $U$  non-negative singular values  $\sqrt{\gamma_1}, \dots, \sqrt{\gamma_U}$  of  $\mathbf{H}$ , sorted in descending order on

the main diagonal. Using this decomposition, we obtain the equivalent model

$$\tilde{\mathbf{y}} = \mathbf{\Gamma}\tilde{\mathbf{x}} + \tilde{\boldsymbol{\eta}}, \quad (4)$$

with  $\tilde{\mathbf{y}} = \mathbf{U}^H\mathbf{y}$ ,  $\tilde{\mathbf{x}} = \mathbf{V}^H\mathbf{x}$  and  $\tilde{\boldsymbol{\eta}} = \mathbf{U}^H\boldsymbol{\eta}$ . This way, the MIMO system from (1) is transformed into  $U$  parallel and non-interfering single-input-single-output (SISO) channels.

The channel capacity of this system is calculated by the sum over all parallel sub-channels, i.e.

$$C = \sum_{u=1}^U \log_2 (1 + \rho\gamma_u), \quad (5)$$

where  $\gamma_u$  are the eigenvalues of  $\mathbf{H}\mathbf{H}^H$ . They equal the square of the singular values of  $\mathbf{H}$ . Since  $\mathbf{H}\mathbf{H}^H$  is positive semi-definite, the eigenvalues are in the range of  $0 \leq \gamma_u \leq \text{tr} \{ \mathbf{H}\mathbf{H}^H \} = \sum_{u=1}^U \gamma_u = UV|a|^2$ . The magnitude of the  $u$ -th singular value in  $\mathbf{\Gamma}$  represents the channel gain of the  $u$ -th equivalent SISO channel or eigenmode.

To explain the condition for which the maximum MIMO channel capacity is achieved, let us rewrite (5) as  $C = \sum_{u=1}^U \log_2 (1 + \rho\gamma_u) = \log_2 \left( \prod_{u=1}^U (1 + \rho\gamma_u) \right)$ . Since the logarithm is monotonically increasing,  $C$  is maximized by maximizing  $\prod_{u=1}^U (1 + \rho\gamma_u)$ . It can be shown by basic algebra that, if the sum of  $U$  non-negative numbers is fixed, their product is maximized for the case where they are all equal. Therefore the MIMO capacity is maximized when all eigenvalues are equal. Since  $\sum_{u=1}^U \gamma_u = UV|a|^2$ , the optimal eigenvalue profile must be  $\gamma_u = V|a|^2 \forall u$ . In this case, a CNR gain of  $V$  and a multiplexing gain of  $U$  is achieved, and (5) yields

$$C_{\text{opt}} = U \log_2 \left( 1 + \rho V |a|^2 \right). \quad (6)$$

From (6), it is clear that the multiplexing gain is limited to  $U$ , i.e. the maximum number of parallel sub-channels of  $\mathbf{H}$ . Therefore, an additional antenna at the link end with  $V$  antennas does not increase the multiplexing gain, but increases the CNR by a factor of  $V + 1$ . However, as long as all  $U$  eigenvalues are equal, the channel capacity is maximized according to (6), and  $\mathbf{H}$  is called an ‘‘optimal MIMO channel’’. For  $M > N$  (respectively,  $M \leq N$ ), all column (row) vectors of  $\mathbf{H}$  are then pairwise orthogonal and have equal norm. The latter is actually always fulfilled for the pure LOS channel matrix since all

<sup>1</sup>To give an example: Assume that one earth station antenna is located at the sub-satellite point while a second earth station antenna has a relative distance to the first earth station antenna of  $3^\circ$  in geographical longitude (corresponds to a distance of approximately 340 km). In this case the relative error is approximately  $2.9 \times 10^{-4}$ . In other words, the magnitude of the amplitude has an error of 0.04 dB at 20 GHz, which can be neglected.

the coefficients have identical magnitude. If  $M = N$ ,  $\mathbf{H}$  is a scaled unitary matrix having orthogonal row and column vectors, i.e.  $\mathbf{H}\mathbf{H}^H = \mathbf{H}^H\mathbf{H} = M|a|^2\mathbf{I}_M$ .

A simple  $2 \times 2$  example of an optimal MIMO channel is  $\mathbf{H} = a \begin{bmatrix} 1 & 1 \\ 1 & e^{-j\pi} \end{bmatrix}$ , which again highlights the need to model the different phase entries of  $\mathbf{H}$ . Here the two transmit signals impinge phase aligned at the first receive antenna, and they exhibit a phase difference of  $\pi$  at the second receive antenna. A phase difference of  $\pi$  corresponds to a difference among the path lengths of  $\lambda_c/2$ . The condition to obtain such channels will be derived in Section II-C, and it will be shown in Section II-D that this condition requires particular spacings between the antennas at the transmitter and the receiver.

Consider now the example where all receive signals at each receive antenna are nearly phase aligned, i.e. the PWM can be applied. All path lengths are approximately equal and the channel matrix is  $\mathbf{H} \approx a \begin{bmatrix} 1 & 1 \\ 1 & 1 \end{bmatrix}$ . This is the so-called ‘‘keyhole channel’’ [22], which provides only one sub-channel or eigenmode. All eigenvalues are zero except of one that is  $\gamma_1 = UV|a|^2$ . The keyhole capacity constitutes the lower capacity bound for MIMO systems and is given as

$$C_{\text{key}} = \log_2 \left( 1 + \rho UV |a|^2 \right). \quad (7)$$

It is used for comparison purposes in the following.

### C. Optimal MIMO Satellite Channels

In this section, the general criterion for ‘‘optimal’’ MIMO satellite channels is derived. We have shown that the pure LOS channel matrix  $\mathbf{H}$  is optimal if all row (or column) vectors in case of  $M \leq N$  (or  $M > N$ ) are pairwise orthogonal. This requirement can be formulated as

$$\begin{aligned} \mathbf{h}_{r,k} \mathbf{h}_{r,l}^H &= 0, k, l \in \{1, \dots, M\}, k > l, \text{ if } M \leq N, \\ \mathbf{h}_{c,k} \mathbf{h}_{c,l}^H &= 0, k, l \in \{1, \dots, N\}, k > l, \text{ if } M > N, \end{aligned} \quad (8)$$

where  $\mathbf{h}_{r,k}$  and  $\mathbf{h}_{c,k}$  denote the  $k$ -th row vector and the  $k$ -th column vector of  $\mathbf{H}$ , respectively. Both conditions in (8) are equivalent, and it is, therefore, sufficient to consider the case  $M \leq N$  in the following. We will see later that the result for  $M > N$  is similar.

Applying (2) to (8) for  $M \leq N$  we obtain<sup>2</sup>

$$\sum_{n=1}^N e^{-j\frac{2\pi}{\lambda_c}(r_{kn}-r_{ln})} = 0, k, l \in \{1, \dots, M\}, k > l. \quad (9)$$

An appropriate choice of the various distances between the transmit and receive antennas is the key to satisfy (9) since the other parameters are constant for all  $N$  phasors.

To find a solution for (9), we first consider the following condition:

$$\sum_{n=1}^N e^{-j\beta(n+\kappa)} = 0, \beta \in \mathbb{R} \setminus \{0\}, \kappa \in \mathbb{R}. \quad (10)$$

The sum in (10) corresponds to the sum of  $N$  terms of a geometric series and can be written as

$$\sum_{n=1}^N p \cdot q^n = p \cdot q \cdot \frac{1 - q^N}{1 - q} = 0, p = e^{-j\beta\kappa}, q = e^{-j\beta}. \quad (11)$$

The condition (10) is satisfied if  $1 = e^{-j\beta N}$  and  $1 \neq e^{-j\beta}$ . The solution that fulfills both constraints is

$$\beta = 2\pi v/N, v \in \mathbb{Z}, \text{ with } v \nmid N, \quad (12)$$

where  $v \nmid N$  means  $v$  must not be a multiple of  $N$ . Using the substitution  $\frac{2\pi}{\lambda_c}(r_{kn} - r_{ln}) = \beta(n + \kappa)$  in (10), we obtain

$$(r_{kn} - r_{ln}) = \lambda_c v_{kl} (n + \kappa_{kl}) / N, k, l \in \{1, \dots, M\}, \quad (13)$$

with  $k > l$ ,  $v_{kl} \in \mathbb{Z}$ ,  $v_{kl} \nmid N$  and  $\kappa_{kl} \in \mathbb{R}$ .

Note that  $v_{kl}$  and  $\kappa_{kl}$  can be different for different value pairs of  $(k, l)$  because the  $N$  phasors in (9) for one particular set of  $(k, l)$  are independent of any other value pair  $(k', l')$ . The solution in (13) is the very general condition to obtain optimal MIMO satellite channels with arbitrary antenna number under LOS conditions. Note that no particular constraints with respect to (w.r.t.) the geometrical arrangement of the antenna elements have been applied so far.

If we assume the antennas are arranged as uniform linear arrays (ULAs), (13) can be simplified to achieve the result reported in [24]. If ULAs at both link ends are applied and a large distance between the transmitter and receiver compared to the array

<sup>2</sup>Please note that we divided (8) by  $|a|^2$  to obtain (9).

dimensions is assumed,<sup>3</sup> it can be revealed through geometrical analysis that

$$(r_{kn+1} - r_{ln+1}) - (r_{kn} - r_{ln}) \approx \text{const.} \quad (14)$$

for  $n \in \{1, \dots, N-1\}$  and  $k, l \in \{1, \dots, M\}$ ,  $k > l$ . Since (14) holds for all combinations of the indices  $k, l, n$  with  $k > l$ , we can set w.l.o.g.  $k = 2$ ,  $l = 1$  and  $n = 1$ . Using (13) in (14) finally yields

$$(r_{22} - r_{12}) - (r_{21} - r_{11}) = v\lambda_c/N, \quad v \in \mathbb{Z}, \quad v \nmid N. \quad (15)$$

This result has first been published in [13] in 2008 for MIMO SATCOM applications. Although the derivation has been slightly different and was limited to  $N = 2$  satellite antennas, (15) tackles the solution presented in [13]. It satisfies (9) under the constraint that ULA geometries are used at both link ends. Moreover, the result remains valid for  $M > N$  by replacing  $N$  with  $M$  on the right hand side of the equation. If the differences between the path lengths satisfy (15), the resulting MIMO LOS channel exhibits the maximum channel capacity according to (6). Condition (15) leads to particular requirements with respect to the positioning of the antenna elements as presented next. Moreover, the analysis shows that the signal phase must be taken into account.

#### D. Optimal MIMO SATCOM Antenna Positioning

In the following, we apply the result of (15) to obtain maximum-capacity MIMO SATCOM links. To this end, we need to calculate the distances between the transmit-receive antenna pairs, which are determined by the geographical locations of the antenna elements on Earth and in space. A set of geometrical design parameters is introduced that exactly defines the geographical locations of the antenna elements. Moreover, the analysis shows that the signal phase must be taken into account. This is fundamentally different from the great bunch of existing publications on MIMO satellite systems, which apply a PWM through narrow antenna spacing and can, therefore, never achieve a higher capacity than keyhole.

All the required parameters are illustrated in Fig. 1. The antenna locations are defined using an

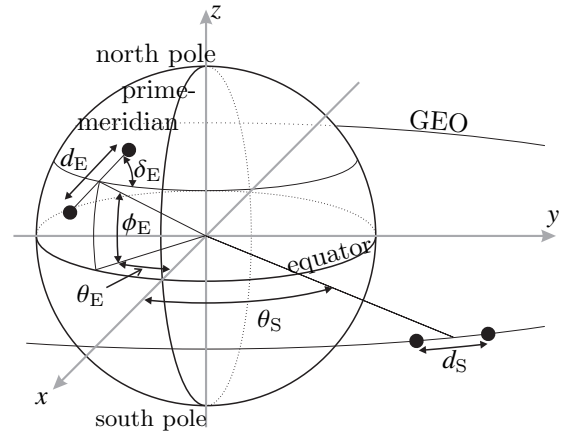


Fig. 1. Parameter definition to describe the antenna positions, exemplary  $M = 2$  earth station antennas and  $N = 2$  satellite antennas are shown

earth centered, earth fixed (ECEF) coordinate system. For the sake of simplicity, the distance between the Earth's center and any point on its surface is set equal to the mean Earth radius  $R_{\oplus} = 6,378.1$  km. Since the distance between the earth station antennas is small compared to  $R_{\oplus}$ , the Earth curvature is neglected. It will be shown later in this section that this simplification has a negligible impact on the optimal design of the MIMO satellite link. The orientation  $\delta_E$  characterizes the angle between the east-west direction and the antenna array. The pair of latitude  $\phi_E$  and longitude  $\theta_E$  specifies the center of the antenna array, and  $d_E$  is the inter-antenna distance. This allows to fully characterize the position of the ground antennas. The positioning vector of the  $m$ -th earth station antenna in three-dimensional Cartesian coordinates is given in (16) at the top of the next page, where  $d_{E,m} = d_E \cdot (m - 1/2 - M/2)$ .

At the satellite, the antennas are considered to be positioned in the equatorial plane. Denoting  $\theta_S$  as the longitude of the center of the antenna array,  $d_S$  as the inter-antenna spacing, and  $R_o = 42,164.2$  km as the ideal GEO radius, the position of the  $n$ -th satellite antenna in three-dimensional Cartesian coordinates is given by

$$\mathbf{a}_{S,n} = [R_o \cos \theta_S - d_{S,n} \sin \theta_S, R_o \sin \theta_S + d_{S,n} \cos \theta_S, 0]^T, \quad (17)$$

with  $d_{S,n} = d_S \cdot (n - 1/2 - N/2)$ . Here, an ideal GEO is assumed, i.e. the eccentricity and inclination of the satellite are negligibly small. The validity of this simplification will be justified in the remainder of

<sup>3</sup>This is a valid assumption for GEO applications since the Earth-to-space distance is at least 35,786.1 km, while the array dimensions are assumed to be not larger than several tens of km.

$$\mathbf{a}_{E,m} = \begin{bmatrix} R_{\oplus} \cos \phi_E \cos \theta_E - d_{E,m} \cdot (\sin \theta_E \cos \delta_E + \sin \phi_E \cos \theta_E \sin \delta_E) \\ R_{\oplus} \cos \phi_E \sin \theta_E + d_{E,m} \cdot (\cos \theta_E \cos \delta_E - \sin \phi_E \sin \theta_E \sin \delta_E) \\ R_{\oplus} \sin \phi_E + d_{E,m} \cdot \cos \phi_E \sin \delta_E \end{bmatrix}, \quad m \in \{1, \dots, M\}, \quad (16)$$

this section.

Based on the previous parametric characterization, the distance  $r_{mn}$  between the  $m$ -th receive antenna and the  $n$ -th satellite transmit antenna is then given by

$$r_{mn} = \|\mathbf{a}_{E,m} - \mathbf{a}_{S,n}\| = r \cdot (1 + \Delta_{mn})^{1/2}, \quad \text{with} \quad (18)$$

$$\Delta_{mn} = 2 (d_{E,m} R_o \alpha - d_{S,n} R_{\oplus} \beta + d_{E,m} d_{S,n} \psi) / r^2 + (d_{E,m}^2 + d_{S,n}^2) / r^2. \quad (19)$$

Here,  $r = \Delta r \cdot r_{\min}$  is the distance between the center of the earth station ULA and the satellite. Moreover,  $r_{\min} = 35,786.1$  km is the minimum satellite-to-Earth distance, which is obtained if the earth station is directly located at the sub-satellite point. The parameter  $\Delta r = (1.42 - 0.42 \cos \phi_E \cos \Delta \theta)^{1/2}$  with  $1 \leq \Delta r \leq 1.16$  describes the relative increase of the satellite-to-earth station distance depending on the geographical latitude  $\phi_E$  and the relative longitude  $\Delta \theta = \theta_E - \theta_S$ . Furthermore, the substitutions  $\alpha = \cos \delta_E \sin \Delta \theta + \sin \phi_E \sin \delta_E \cos \Delta \theta$ ,  $\beta = \cos \phi_E \sin \Delta \theta$ , and  $\psi = \sin \phi_E \sin \delta_E \sin \Delta \theta - \cos \delta_E \cos \Delta \theta$  have been defined.

Approximating the square root in (18) by its second degree Taylor polynomial derived around  $\Delta_{mn} = 0$  provides

$$r_{mn} \approx r \cdot \left(1 + 1/2 \cdot \Delta_{mn} - 1/8 \cdot \Delta_{mn}^2\right). \quad (20)$$

Using (20) with (19) in (15) results in

$$d_S d_E / r \cdot \left(\psi + 0.21 \alpha \beta / \Delta r^2\right) \approx v \cdot \lambda_c / N, \quad v \in \mathbb{Z}, \quad v \nmid N. \quad (21)$$

With respect to the desired accuracy of the Taylor approximation in (20), we require the absolute value of the total error  $|\Delta R|$  of the left hand side of (21) to be much smaller than the carrier wavelength  $\lambda_c$ . In particular, the residual shall be a fraction of the carrier wavelength only, for example  $|\Delta R| \leq 1/100 \cdot \lambda_c$ , in order to obtain reliable results. Computer simulations have shown that in all practically relevant cases  $|\Delta R| \leq 3.8 \times 10^{-6}$  m, which is sufficiently small to support carrier frequencies of more than

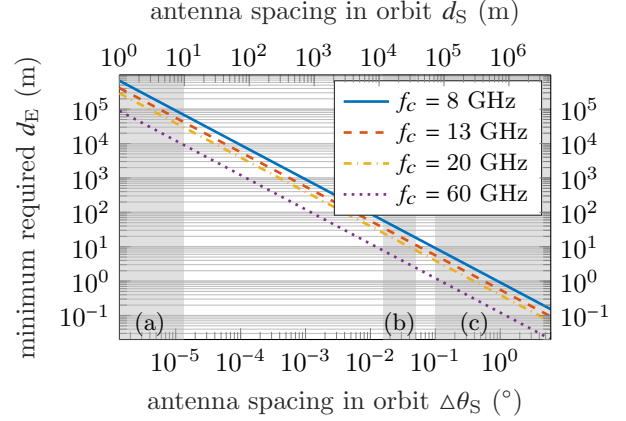


Fig. 2. Minimum spacing  $d_E$  versus antenna spacing in orbit, shaded areas indicate useful ranges related to the categories: (a) single-satellite applications, (b) collocated satellite applications, (c) multiple-satellite applications

100 GHz.

As expected, the two key parameters of the solution in (21) are the antenna spacing  $d_E$  on Earth and  $d_S$  in orbit. The spacing required is linearly proportional to the transmitter-receiver distance  $r$  and the wavelength, i.e.  $d_S d_E \propto r \lambda_c$ . Since  $r \geq 35,786.1$  km, comparably large antenna spacings  $d_S, d_E$  are required to satisfy (21).

The minimum array dimensions are generally obtained if both antenna arrays are in broadside and the earth station is at the sub-satellite point. In this case, we have  $\psi = -1$ ,  $\alpha = \beta = 0$ , and  $r = r_{\min}$ . The minimum spacing of the earth station array becomes  $d_E = r_{\min} \lambda_c / (N d_S)$  if we set  $v = 1$ . Smaller values of  $d_E$  lead to severe spatial interference because the receive array is no longer capable to spatially resolve each transmit antenna. All transmit signals can no longer be distinguished at the receiver and the MIMO channel converges to the *keyhole channel* with  $\mathbf{H} \approx a \begin{bmatrix} 1 & 1 \\ 1 & 1 \end{bmatrix}$ . A similar limit is also known as the Rayleigh criterion describing the resolution limit of optical systems.

Fig. 2 shows the relation between  $d_E$  and the antenna spacing in orbit for different carrier frequencies. Since a wide range of values is provided the curves are shown in double-logarithmic scale. For large antenna separations

in orbit, it is convenient to define the orbital separation  $\Delta\theta_S$ , given in degrees on the lower x-axis, while the upper x-axis shows  $d_S$  in meters. The values are valid for  $M = N = 2$ , but can easily be scaled to higher antenna numbers using the relation  $d_E \propto 1/N$ . Since  $\psi = -1$  and  $\alpha = \beta = 0$ , the antenna arrays are in broadside orientation, i.e.  $\delta_E = 0^\circ$ , and  $\Delta\theta = 0^\circ$ . As indicated by the shaded areas in Fig. 2, we propose to classify MIMO SATCOM systems into three basic categories. For each category a particular range of antenna spacings in orbit is basically feasible as follows:

**(a) Single-Satellite Applications:** All MIMO antenna elements are on a single-satellite and the useful antenna spacing is in the range of  $1 \text{ m} \leq d_S \leq 10 \text{ m}$ . A very promising and completely novel system proposal of this category is presented in the remainder of this paper.

**(b) Collocated Satellite Applications:** Multiple satellites occupy a single orbital slot. Each satellite has one MIMO antenna element. A sufficient minimum separation between the spacecrafts must be ensured to account for inaccuracies of the tracking system and the thrusters [25]. The upper bound is the station keeping window, which is typically  $\pm 0.05^\circ$  in longitude. We assume practically feasible antenna spacings to be in the range of  $0.014^\circ \leq \Delta\theta_S \leq 0.05^\circ$  (or equivalently  $10 \text{ km} \leq d_S \leq 40 \text{ km}$ ). Applications of this category are very similar to the single-satellite case but at increased complexity since novel spacecraft co-location strategies are required.

**(c) Multiple-Satellite Applications:** Multiple satellites with one MIMO antenna each are located at different orbit positions resulting in a spacing of  $\Delta\theta_S \geq 0.1^\circ$ . This category of applications requires non-directional antennas at the ground segment because directional antennas cannot point at different orbital slots at the same time. As a promising application, UHF SATCOM has been proposed in [26], and UHF MIMO satellite channel measurements reported in [16] have shown a significant increase of the channel capacity.

Fig. 2 emphasizes which spacing between the earth station antennas is at least required depending on the MIMO SATCOM category considered. In the single-satellite case, the minimum antenna spacing on Earth is approximately between 10 km and 100 km. Smaller antenna spacings  $d_E$  require larger

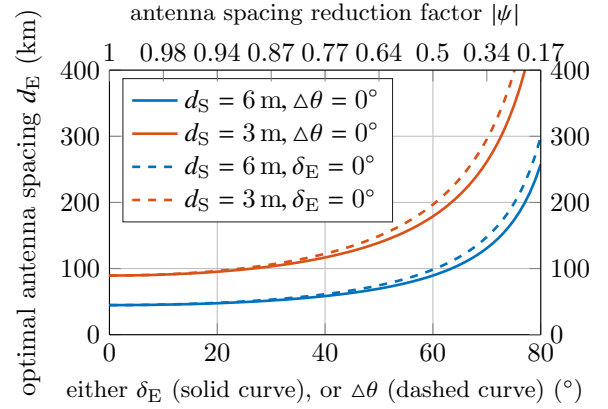


Fig. 3. Optimal antenna spacing  $d_E$  as a function of ULA orientation angle  $\delta_E$  or relative longitude  $\Delta\theta$  and  $\psi$ ,  $M = N = 2$ ,  $\phi_E = 0^\circ$ ,  $f_c = 20 \text{ GHz}$  (single-satellite applications)

spacings in the orbit, leading to collocated satellite applications or to multiple-satellite applications. Note that larger but still optimal values for  $d_E$  can be obtained if  $\nu > 1$ ,  $\nu \nmid N$ , is chosen because the optimal antenna spacing scales with  $\nu\lambda_c/N$ ,  $\nu \nmid N$ .

The term  $(\psi + 0.21\alpha\beta/\Delta r^2) \in [-1, +1]$  in (21) can be interpreted as a *reduction factor* because it apparently reduces the actually needed antenna spacings  $d_E$  and  $d_S$ , depending on the parameters  $\delta_E$ ,  $\Delta\theta$  and  $\phi_E$ . If the earth station ULA and the satellite ULA are not in broadside, we get  $|\psi + 0.21\alpha\beta/\Delta r^2| < 1$ , and the antenna spacing has to be increased accordingly to still satisfy (21).

This required adjustment is shown in Fig. 3 with respect to  $d_E$ . Two  $2 \times 2$  cases are considered: First, the earth station ULA is rotated by  $\delta_E$  while the angles  $\phi_E = \Delta\theta = 0^\circ$  are fixed. This means that the earth station ULA is located at the sub-satellite point. This case corresponds to the solid curves, and the lower x-axis shows  $\delta_E$  in degrees. The second case corresponds to the dashed curves and the relative longitude  $\Delta\theta$  is increased while  $\phi_E = \delta_E = 0^\circ$  are fixed. In both cases  $\alpha = \beta = 0$  and, thus,  $|\psi + 0.21\alpha\beta/\Delta r^2| = |\psi|$  as shown on the upper x-axis. In all cases, comparably large angular values of  $\delta_E$  and  $\Delta\theta$  are allowed for which the optimal spacing  $d_E$  remains approximately constant. This is due to the fact that the increment of  $d_E$  relates to the cosine of the respective angles.

Taking the solid blue curve for  $d_S = 6 \text{ m}$  as an example, the optimal  $d_E$  has to be increased by only about 7 km compared to the minimum value of 50 km for  $\delta_E = 30^\circ$ , since  $1/|\psi| \cdot d_E = 1/0.87 \cdot$



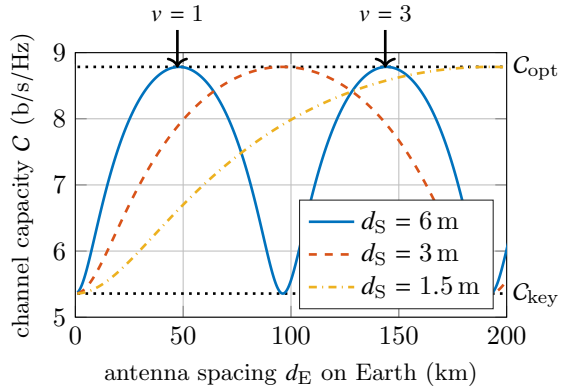


Fig. 4. Capacity vs. antenna spacing on Earth for various antenna spacing at the satellite (single-satellite applications)

50 km = 57 km. The rotation of  $\delta_E = 30^\circ$  results in a displacement of the earth station antennas by 12.5 km to the North and to the South.

The increment of the dashed curves is slightly higher because the transmitter-receiver distance  $r$  also increases with increasing  $\Delta\theta$ . However, assuming a fixed optimal earth station spacing of  $d_E = 50$  km at  $\Delta\theta = 0^\circ$  (blue dashed curve in Fig. 3) and accepting 10 km deviation from this optimum spacing to account for practical implementation constraints, a very large part of the GEO arc of more than  $\Delta\theta = \pm 30^\circ$  can be used. In other words, once an optimal setup has been implemented in terms of a ground station installation, it can be used for a wide range of satellite positions without significant capacity degradation. Therefore, the presented design constraint does not at all impose a flexibility disadvantage to the system.

### E. Sensitivity Discussion

To estimate the degradation of the MIMO capacity if the antennas are not optimally spaced, simulation results of  $C$  as a function of  $d_E$  are shown in Fig. 4. The curves relate again to the  $2 \times 2$  downlink at 20 GHz. A receive CNR of  $10 \log_{10} \rho |a|^2 = 10$  dB is assumed. First, all curves show the expected periodic behavior. Each capacity maximum corresponds to one particular value of  $v$ .

For example, the first and second maximum of the blue solid curve at approximately 50 km and 150 km correspond to  $v = 1$  and  $v = 3$ , respectively. The keyhole capacity is obtained for  $v = 2$  at 100 km because in this case  $v$  is a multiple of  $N = 2$ . Moreover, a large deviation of the optimal

spacing  $d_E$  on Earth is indeed possible without a significant loss of  $C_{\text{opt}}$ . Taking again the blue solid curve for  $d_S = 6$  m as an example,  $\pm 10$  km around the first optimal value of 50 km is allowed to still obtain 8.6 b/s/Hz (the maximum is 8.8 b/s/Hz). This is approximately 98% of  $C_{\text{opt}}$ . The curves reveal that large deviations in all directions even in the kilometer-range can be accepted and still close-to-maximum capacity values are obtained.

The same is true regarding possible displacements of the satellite in the GEO. Since orbit perturbations cause apparent displacements of the satellite w.r.t. its ideal geostationary position, the inclination and eccentricity vary over time. The amplitude of the overall orbital motion is specified by the station-keeping box, whose limits are usually  $\pm 0.05^\circ$  in longitude and latitude and  $4 \times 10^{-4}$  in eccentricity [19]. In the single-satellite case, movements by this order of magnitude can generally be neglected. A displacement of the satellite in geographical longitude by  $0.05^\circ$  from its optimal position results in a variation of the relative longitude, i.e.  $\Delta\theta \pm 0.05^\circ$ .

The effect upon the optimal spacing of the earth station antennas has already been discussed by means of the dashed curves in Fig. 3. The slope of the curves increases for larger values of the relative longitude  $\Delta\theta$ . Taking  $\Delta\theta = 80^\circ$  as an example, an adjustment of the earth station antenna spacing of  $8.2 \times 10^{-4}$  m would be required in order to compensate the satellite's longitude drift. Such values are far too small to have a remarkable impact on the channel capacity, so that the related effects can be neglected.

In short, we conclude that for single-satellite applications:

- The required positioning accuracy of the earth station antennas is manageable in practice. Several kilometers of antenna displacements in each direction are possible while still achieving very high, nearly optimal capacities.
- Satellite movements in the station-keeping window can be neglected.
- A large part of more than  $\pm 30^\circ$  of the GEO arc can be covered with the same earth station installation while limiting the capacity degradation to less than 2%.

The measurements reported in [15] ultimately

confirm the presented theory.<sup>4</sup> To conclude this introductory section about the basics of spatial MIMO over LOS satellite channels, atmospheric impairments and the issue of differential signal delays need to be discussed.

### F. Atmospheric Impairments and Further Aspects

1) *Atmospheric Impairments:* In the frequency bands above 10 GHz, the main radiowave propagation impairments originate from the troposphere and include attenuation effects as well as phase disturbances [27]. An amplitude attenuation decreases the signal power, resulting in a lower CNR for the affected antenna. Such a loss entails a capacity degradation similar to what would be observed in a SISO system suffering from the same attenuation [28]. On the other hand, the impairments of the signal phase might affect the optimal phase relations within the channel matrix  $\mathbf{H}$  and disturb the optimal eigenvalue profile. Fortunately, the channel capacity is not changed if the signal paths originating from the same antenna experience identical phase impairments [28]. This latter property can be reasonably considered to be verified in practice.

The assumption of identical phase impairments is based on the geometrical analysis of an optimal MIMO satellite link where the horizontal separation in the troposphere of two LOS paths  $r_{m1}$  and  $r_{m2}$  is very small. In fact, the example in [28, eq. (7)] reveals a horizontal separation of less than 1 cm. This theoretical assumption has been verified through interferometric measurements in the Ku-Band at 12.5 GHz reported in [14]. The results prove that differential phase disturbances between neighboring LOS paths can be neglected. Moreover, the long-term measurements have also shown that, once an optimal MIMO satellite link has been established, the maximum MIMO capacity can be obtained sustainably. It is, therefore, reasonable to model a common attenuation and phase shift for signal paths stemming from or arriving at the same earth station antenna.

The atmospheric impairments for the  $m$ -th earth station antenna are expressed as  $\zeta_m = |\zeta_m| \cdot e^{-j\xi_m}$ , where  $|\zeta_m| \in [0, 1]$  and  $\xi_m \in [-\pi, \pi[$  represent re-

spectively the additional amplitude attenuation and the phase shift. The attenuation in dB is obtained as

$$A_m = -20 \cdot \log_{10}(|\zeta_m|). \quad (22)$$

The LOS free space channel coefficient in (2) is, thus, extended to  $\tilde{h}_{mn} = h_{mn} \cdot \zeta_m$ . It follows for the impaired channel transfer matrix

$$\tilde{\mathbf{H}} = \mathbf{D} \cdot \mathbf{H}, \quad (23)$$

with  $\mathbf{D} = \text{diag}\{\zeta_1, \dots, \zeta_M\}$ . The influence of the weather impairments on the MIMO feeder link of an HTS system will be analyzed in Section III.

2) *Differential Signal Delays:* A known issue of MIMO satellite links is the large difference in the propagation delay between the LOS paths [29]. The time of arrival of the MIMO signals at the receiving antennas can vary by hundreds of a symbol duration because of the large antenna spacing. This results in an asynchronous reception of those symbols which form a part of a single code word.

To tackle this issue, a single-carrier frequency domain equalization (SC-FDE) concept has been applied in [30]. By using a sufficiently long guard interval, the different arrival times of the symbols can be compensated. The unavoidable loss in bandwidth efficiency depends on the length of the guard interval in relation to the frame length and usually does not exceed 5% [30]. An advantage of SC-FDE compared to other waveforms, which also rely on the use of a guard interval like orthogonal frequency division multiplexing, is its very low peak-to-average power ratio. However, modern waveforms currently discussed as 5G candidates [31] are also potentially suitable to address these differential propagation delays in future systems.

## III. MIMO HTS SYSTEM PROPOSAL

Relying on the result of Section II, we now apply the MIMO concept to an HTS system. With an HTS system, the limitations of a broadcast scenario can be tackled and multiple users can be served with individual data streams. HTS systems represent the most recent and powerful satellite architecture for high-data rate unicast and multicast communications. We will show how greatly these systems can benefit from spatial multiplexing in both their uplink and their downlink, to maximize the sum throughput. The considered FSS scenario belongs to the class of single-satellite MIMO applications

<sup>4</sup>Since the measurement setups have been fairly complex, we do not repeat the results here, but we encourage the reader to take note of this practical field trial.

since one HTS equipped with several antennas will be assumed.<sup>5</sup>

We recall that the objective of the considered illustrative example is to show the tremendous performance gain of a MIMO HTS system in terms of data rate if the MIMO LOS system design approach from the previous section is considered. To this end, the proposed HTS system architecture with a MIMO feeder link and a MU-MIMO downlink is presented first together with the equivalent baseband model. The system model will be used in Section III-E to design the precoding strategies aimed at improving the spectral efficiency of the system. Section III-D describes the scheduling approach based on the algorithm in [17] that allocates the resources to individual households. Simulation results are provided in Section IV to finally assess the system performance in terms of sum rates in comparison to the state-of-the-art.

### A. System Description

The MIMO HTS system architecture is depicted in Fig. 5. Here we concentrate on the forward link, i.e. the link from the gateway to the users. Since a complete transmission chain with the uplink and the downlink is now considered, the mathematical notation to distinguish both parts will be adapted accordingly.

1) *MIMO Feeder Uplink*: The Earth portion of the MIMO feeder link consists of  $N = 2$  gateway antennas, separated by several kilometers (30 km to 50 km) and inter-connected via a central processing unit which supervises the generation of the transmit signals. Time and phase synchronization of the antennas is ensured. RF-over-fiber transport can, for example, be used for this purpose [33]. This technology has been successfully applied at the NASA deep space network, where antennas separated by more than 10 km must be synchronized for deep space communications. In the following, it is assumed that the inter-connection between the gateway antennas is perfect.

At the satellite,  $Z_r = 2$  receive antennas are positioned in the orbital plane  $d_S = 3$  m apart, constituting the receive array of the MIMO feeder

link. To operate this feeder link, the bands 42.5-43.5 GHz and 47.2-50.2 GHz are exploited such that a total bandwidth of 4 GHz per polarization state is available. The receive antennas cover the same geographical region centered in the middle of the gateway array, and the assumption is made that their beamwidth is sufficiently large. In that way, the antennas are relatively close to the beam center, and the receive antenna gain is maximum for all transmit-receive antenna links.

The satellite payload relies on a bent-pipe architecture with cross-strapping from the V-band feeder uplink to the Ka-band user downlink. No signal processing is considered in the payload to keep the satellite complexity low. Nevertheless, we observe that some sample-based signal processing could be envisioned. An architecture supporting digital transparent processing, known as *digital bent-pipe*, would then be required. We will leave the further development of this possibility for future research. Some hints can be found also in [34], [35].

It has to be noted that, to support the large aggregate user link bandwidth of a HTS system, several tens of spatially separated feeder links with a full reuse of the available frequency band are actually required in practice [36]. To this end, several feeds are installed on the receive reflectors in order to cover different sites on Earth. In this case, an advantage of the MIMO approach lies in the fact that the necessary number of spatially separated links can be halved compared to state-of-the-art SISO links (e.g. 15 MIMO feeder links instead of 30 SISO links) [32]. Meanwhile, the total number of active gateway antennas in the system remains the same since two gateway antennas per feeder link are now used.

The resort to MIMO feeder links can be intuitively seen as a solution to rearrange the antennas such that part of the interference between typical SISO feeder links is transformed into an information-bearing signal using spatial multiplexing. With a MIMO-based architecture, the angular separation of the different feeder links in a given region of deployment (e.g. Northern America) can indeed be increased to improve the beam isolation. In general, a distance of several hundreds of kilometers is required between the sites to guarantee sufficiently high carrier to interference ratios (CIRs).

Here, the uplink part of the considered forward link consists of a single feeder link because the

<sup>5</sup>The architecture of spatial MIMO in the feeder link of an HTS scenario has also been chosen in [32] and [20] for feeder link performance analyses that are out of scope of this paper.

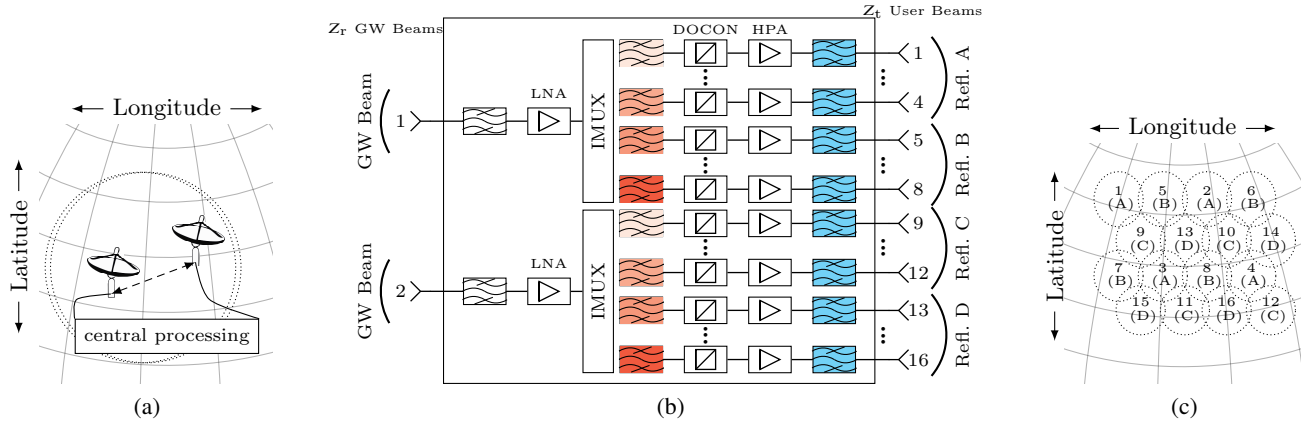


Fig. 5. Proposed system architecture: (a) Two spatially separated gateway antennas are fed with signals by a common gateway station (central processing). (b) Schematic diagram of the proposed payload: Both gateway (GW) beams share a common frequency resource (V-band). The payload is designed to translate all incoming frequency bands to the same frequency band in the Ka-band in order to enable FFR. The colors of the bandpass filters indicate the corresponding frequency range according to Fig. 6. (c) Geographical illustration of the 16 spot beam footprints. The dotted lines represent the 3 dB contours of the multiple beams. The source feed and reflector are labeled inside every footprint.

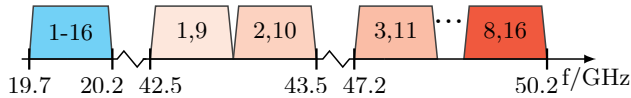


Fig. 6. Single polarization frequency plan for the up- and the downlink: FFR is applied in the downlink (Ka-band), so all 16 beams share a common frequency band. The multiplexing gain enables a parallel transmission of two feed signals by the feeder link within the same frequency segment of the V band. The numbers indicate the corresponding beam according to Fig. 5

goal of the example is simply to illustrate how spatial multiplexing can be realized in a given link. The downlink of the studied HTS system will be dimensioned such that its sum user link bandwidth equals the sum bandwidth that can be supported by its uplink.

2) *Multibeam Downlink*: The downlink part of the HTS system is made of  $Z_t = 16$  Ka-band user beams delivering different data contents to fixed single antenna user terminals (UTs). On the satellite a single-feed-per-beam (SFPB) architecture with  $Z_{\text{refl}} = 4$  multibeam reflectors is considered. The reflectors are geometrically arranged as a uniform circular array with a diameter of 3 m.

On Earth a total of  $K_{\text{tot}}$  user terminals (UTs) are uniformly distributed over the area covered by the  $Z_t$  beams. These UTs are, for example, conventional single-antenna installations on a roof top of a building to serve households with individual data traffic. The comparison in the results section will be made to the conventional FR4 scheme where the

same distribution of  $K_{\text{tot}}$  customers is assumed. This ensures a fair comparison between both schemes and allows a general conclusion from the simulation results. These results can be further extended to other user distributions, scheduling approaches or precoder designs from the literature, e.g. [37], [38].

A downlink bandwidth of 500 MHz within the range of 19.7-20.2 GHz is available for the entire service zone. Since an FFR scheme is addressed, this frequency band is jointly utilized by all beams.

It is known that the achievable multiplexing gain offered by MU-MIMO is limited by the number of channel inputs. Only a group of up to  $Z_t = 16$  UTs can be served simultaneously via space division multiple access (SDMA). Thus, the user downlink forms at most a  $16 \times 16$  MIMO channel. Since  $K_{\text{tot}} \gg Z_t$ , additional user scheduling is necessary to build groups of UTs that will be served in different orthogonal *resource blocks*. These different resource blocks can be, for example, separate time or frequency slots based on a time division multiple access (TDMA) or frequency division multiple access (FDMA) scheme, respectively. Our approach to schedule the  $K_{\text{tot}}$  users will be explained in more detail in Section III-D.

## B. Channel Model

1) *MIMO Feeder Uplink*: The MIMO feeder link channel is modeled in the equivalent baseband using

a block diagonal matrix

$$\tilde{\mathbf{H}}_{\mathbf{u}} = \text{diag} \left\{ \tilde{\mathbf{H}}_{\mathbf{u},1}, \dots, \tilde{\mathbf{H}}_{\mathbf{u},\frac{Z_t}{2}} \right\} \in \mathbb{C}^{Z_t \times Z_t}, \quad (24)$$

where  $\tilde{\mathbf{H}}_{\mathbf{u},l}$  is a  $2 \times 2$  channel matrix between the  $N = 2$  gateway antennas and the  $Z_r = 2$  satellite receive antennas. The index  $l$  distinguishes the  $Z_t/2$  different center frequencies required due to the use of FDMA in addition to SDMA in the feeder uplink. Each entry  $\tilde{h}_{l,zn}^{(u)}$  corresponds to the channel coefficient from the  $n$ -th gateway antenna to the  $z$ -th satellite receive antenna at the  $l$ -th center frequency and takes both the free space propagation and the atmospheric impairments into account.

Similarly to (23), the matrix  $\tilde{\mathbf{H}}_{\mathbf{u},l}$  can accordingly be expressed as

$$\tilde{\mathbf{H}}_{\mathbf{u},l} = \mathbf{H}_{\mathbf{u},l} \cdot \mathbf{D} \odot \mathbf{G}_{\mathbf{u}}, \quad (25)$$

with  $\mathbf{H}_{\mathbf{u},l} \in \mathbb{C}^{2 \times 2}$ , the MIMO LOS channel matrix whose free space propagation coefficients are determined according to (2). Again, the matrix  $\mathbf{D} \in \mathbb{C}^{2 \times 2}$  is a diagonal matrix modeling the atmospheric impairments experienced by the gateway antennas. We observe that, in contrast to (23), the multiplication with the matrix  $\mathbf{D}$  is performed on the right-hand side since an uplink channel is now considered. The atmospheric impairments for the  $n$ -th earth station should thus affect the  $n$ -th column of  $\tilde{\mathbf{H}}_{\mathbf{u},l}$ .

As already mentioned, rain attenuation represents a severe impairment in the Q/V band and imposes strong constraints on the link budget. It has motivated the development of gateway diversity schemes to ensure system availability [11], [39]–[41]. In the sequel, the assumption is made that rain attenuation is the only weather impairment affecting the receive power in the feeder link. Other types of fading effects can indeed be compensated by an uplink power control scheme. In the results section, the proposed MIMO feeder link will be evaluated for different rain attenuations  $A_1$  at the first gateway antenna given a fixed  $A_2$  at the second antenna.

The elements of matrix  $\mathbf{G}_{\mathbf{u}} \in \mathbb{C}^{2 \times 2}$  model the normalized radiation patterns of the satellite receive antennas. They can be calculated as [42]

$$g_{zn}^{(u)} = J_1(u_{zn})/2u_{zn} + 36J_3(u_{zn})/u_{zn}^3, \quad (26)$$

with  $u_{zn} = \pi D/\lambda_c \sin(\vartheta_{zn})$ , and  $J_1(u_{zn})$  and  $J_3(u_{zn})$  being the Bessel functions of first kind and order one and three, respectively. We assume the same diameter  $D$  for all satellite receive antennas, and  $\vartheta_{zn}$

is the off-axis angle of the  $z$ -th beam's boresight to gateway antenna  $n$ .

In order to take the best advantage of spatial multiplexing in the feeder link, the LOS uplink channel matrix  $\mathbf{H}_{\mathbf{u},l}$  will be designed according to the criterion (21). More precisely, the antenna geometry in the feeder link will be optimized such that a scaled unitary matrix  $\mathbf{H}_{\mathbf{u},l}$  is obtained. It will be shown that, in this case, the sum achievable rate of the HTS system is maximized.

2) *Multibeam Downlink*: In case of FFR, an arbitrary UT can potentially receive signal portions from all feeds. Therefore, the downlink channel  $\tilde{\mathbf{H}}_{\mathbf{d}}$  between the  $Z_t$  feeds and a group of  $K$  UTs is modeled as a densely populated matrix

$$\tilde{\mathbf{H}}_{\mathbf{d}} = \mathbf{H}_{\mathbf{d}} \odot \mathbf{G}_{\mathbf{d}} \in \mathbb{C}^{K \times Z_t}. \quad (27)$$

Here,  $\mathbf{H}_{\mathbf{d}} \in \mathbb{C}^{K \times Z_t}$  denotes the channel matrix that models the free space propagation according to (2) between the  $Z_t$  feeds and the  $K$  households, which are simultaneously served with data in one recourse block. Equivalent to the uplink, the matrix  $\mathbf{G}_{\mathbf{d}} \in \mathbb{C}^{K \times Z_t}$  describes the radiation patterns of the downlink multibeam antennas. The element  $[\mathbf{G}_{\mathbf{d}}]_{k,z} = g_{kz}^{(d)}$  denotes the normalized antenna gain from beam  $z$  to user  $k$ . It is calculated using (26) by an appropriate choice of the antenna parameters.

Similar to the feeder link channel, we are seeking to design an optimal downlink channel matrix  $\tilde{\mathbf{H}}_{\mathbf{d}}$ , in which all row vectors are pairwise orthogonal. In this case the channel capacity is maximized according to (6). In contrast to the feeder link, the locations of the user antennas are arbitrary and an analytical condition as presented in (21) cannot be applied here to derive optimal downlink matrices  $\tilde{\mathbf{H}}_{\mathbf{d}}$ . To this end, a novel user grouping algorithm has been developed in [17], which addresses in particular the construction of downlink matrices  $\tilde{\mathbf{H}}_{\mathbf{d}}$  with pairwise orthogonal row vectors. We will apply and extend this algorithm to our HTS system proposal. It will be briefly recapped in Section III-D. The major difference of our approach compared to the state-of-the-art is reflected in the fact, that the condition of pairwise orthogonality inherently uses the signal phase as a design criterion whereas the great bunch of published work neglects the signal phase (see for example [43] and references therein).

### C. MIMO HTS System Model

The equivalent baseband model of the HTS system under study is now introduced. Imperfections such as the non-linearities of the power amplifiers, phase noise, or differential delay and phase among multiple pathways in the satellite payload are assumed to be perfectly compensated using a calibration method [44]. This correction guarantees that the downlink signals are phase-coherent to enable the feasibility of MU-MIMO precoding.

Please note that, to enable the pre-processing of the transmit signals in the gateways, channel state information (CSI) about the uplink and downlink MIMO channels is necessary. To obtain this CSI, existing channel sounding strategies can be applied to estimate the amplitude and phase of the channel matrices  $\tilde{\mathbf{H}}_{u,l}$  and  $\tilde{\mathbf{H}}_d$ . One solution consists, for example, in the transmission of orthogonal training sequences like the constant amplitude zero auto-correlation (CAZAC) sequence [45] in the forward link. Applying the method as proposed in [15], the phase and amplitude information of the channel coefficients in  $\tilde{\mathbf{H}}_{u,l}$  and  $\tilde{\mathbf{H}}_d$  can be estimated via a cyclic cross-correlation of the signal received by the UTs with the known sequence. This information can be fed back to the gateways via the return link to enable the pre-processing of the transmit signals. A small part of the available resources in the system must, therefore, be reserved for the transmission of a training sequence and the estimation of the channel. However, this is not specific to the approach presented here but applies to all types of precoding schemes for multibeam satellites.

We assume ideal CSI about the uplink and downlink MIMO channels in the sequel. It is known that the system performance degrades if the CSI is imperfect or outdated. The performance of different precoding schemes with imperfect CSI has been investigated in the literature, e.g. in [46], [47], and the interested reader is kindly referred to these papers and the references therein.

Fig. 7 shows a block diagram of the transmission chain with the associated notations. For the sake of a compact notation, time indices are neglected in the sequel. Let

$$\mathbf{s} = [s_1, \dots, s_K]^T \in \mathbb{C}^{K \times 1} \quad (28)$$

be the vector of data symbols to be transmitted in a given time slot to a group of  $K$  non-cooperative

single-antenna UTs, where  $s_k$  is the symbol for the  $k$ -th user. Please note that a pure unicast scenario is considered and that, therefore,  $s_k$  can be different for different  $k$ . These symbols are chosen from a constellation alphabet<sup>6</sup>  $\mathbb{A}$  with unit variance, and are uncorrelated such that  $\mathbb{E}\{\mathbf{s}\mathbf{s}^H\} = \mathbf{I}_K$ .

In the central processing unit of the gateway, a linear transformation of the data vector  $\mathbf{s}$  is performed using a precoding matrix  $\mathbf{B} \in \mathbb{C}^{Z_t \times K}$ . This matrix aims to mitigate the interference between the symbols transmitted in the same frequency channel in the uplink as well as in the downlink. Moreover, denoting  $P_u$  the maximum effective isotropic radiated power (EIRP) per gateway antenna, the following condition must be fulfilled

$$\text{tr}\{\mathbf{B}^H \bar{\mathbf{Q}}_n \mathbf{B}\} \leq P_u, \quad n = 1, 2. \quad (29)$$

The matrix  $\bar{\mathbf{Q}}_n = \text{diag}\{\mathbf{Q}_n, \dots, \mathbf{Q}_n\}$  is a  $Z_t \times Z_t$  block diagonal matrix where  $\mathbf{Q}_n$  is a  $2 \times 2$  matrix containing zeros in all entries except for the  $n$ -th diagonal element which is equal to 1. That is, in  $\bar{\mathbf{Q}}_1$  all odd and in  $\bar{\mathbf{Q}}_2$  all even diagonal entries are 1 while the remaining entries are zero. Condition (29) corresponds to a per-antenna power constraint. It is required since the gateway antennas are equipped with their own high power amplifier (HPA).

After the transmission over the MIMO feeder link, the symbols received by the satellite are

$$\mathbf{y}_u = [y_{u,1}, \dots, y_{u,Z_t}]^T = \tilde{\mathbf{H}}_u \mathbf{B} \mathbf{s} + \boldsymbol{\eta}_u. \quad (30)$$

The vector  $\boldsymbol{\eta}_u = [\eta_{u,1}, \dots, \eta_{u,Z_t}]^T$  is the vector of uplink circularly-symmetric complex Gaussian noise and is uncorrelated with the data symbols. In the sequel, the variance per real dimension of the complex uplink noise process is equal for all  $Z_t$  receive branches and is denoted by  $\sigma_{\eta_u}^2$ .

In the satellite payload, the coefficient  $a_S$  models the amplification of the HPAs. The vector of channel inputs to the downlink is then given by

$$\mathbf{x}_d = [x_{d,1}, \dots, x_{d,Z_t}]^T = a_S \cdot \tilde{\mathbf{H}}_u \mathbf{B} \mathbf{s} + a_S \cdot \boldsymbol{\eta}_u \quad (31)$$

with  $x_{d,z}$  being the downlink signal transmitted by the  $z$ -th feed. The downlink EIRP in each beam should not exceed a maximum value  $P_d$  such that

$$[\mathbf{R}_{\mathbf{x}_d}]_{z,z} \leq P_d, \quad z \in \{1, \dots, Z_t\}, \quad (32)$$

where  $\mathbf{R}_{\mathbf{x}_d} = \mathbb{E}\{\mathbf{x}_d \mathbf{x}_d^H\}$  is the autocorrelation matrix

<sup>6</sup>Modulations are chosen according to the DVB-S2X standard [7].

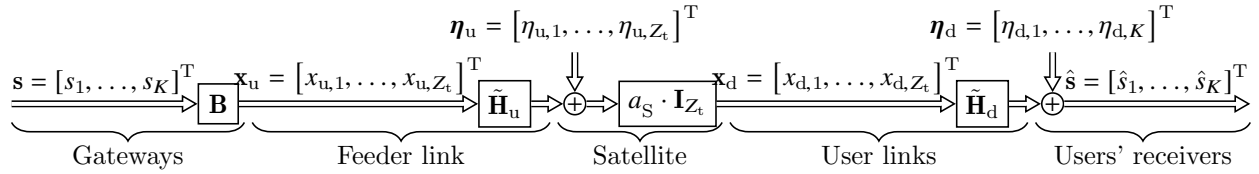


Fig. 7. Block diagram of the transmission chain

of  $\mathbf{x}_d$ . The gain  $a_S$  is consequently chosen to fulfill the constraint (32) with equality for at least one of the feeds. In other words, at least one downlink beam provides the maximum downlink EIRP  $P_d$  while the EIRP of the remaining beams can be lower or, in the best case, equal to  $P_d$ .

We note that the modeling of the satellite through a simple amplification coefficient follows from the assumption of an analog transparent architecture. In the case of a *digital bent-pipe*, a sample-based processing of the signals could be envisioned. The satellite payload would then be modelled by a non-diagonal relaying matrix  $\mathbf{F} \in \mathbb{C}^{Z_t \times Z_t}$ .

In the user links, the receive symbols are

$$\hat{\mathbf{s}} = [\hat{s}_1, \dots, \hat{s}_K]^T = a_S \cdot \tilde{\mathbf{H}}_d \tilde{\mathbf{H}}_u \mathbf{B} \mathbf{s} + a_S \cdot \tilde{\mathbf{H}}_d \boldsymbol{\eta}_u + \boldsymbol{\eta}_d, \quad (33)$$

where  $\boldsymbol{\eta}_d = [\eta_{d,1}, \dots, \eta_{d,K}]^T$  is the vector of downlink circularly-symmetric complex Gaussian noise. This noise is uncorrelated with both the data symbols  $\mathbf{s}$  and the uplink noise  $\boldsymbol{\eta}_u$ . Assuming similar receiving equipment for all households, the variance per real dimension of the noise process at each UT is identical and represented by  $\sigma_{\eta_d}^2$ .

We define the receive CNR at the beam center as

$$\text{CNR}^{\text{bc}} = a_d^2 \cdot P_d / (2\sigma_{\eta_d}^2), \quad (34)$$

where  $a_d$  is the free space downlink gain as defined in (2).

#### D. User Scheduling

As stated before, only up to  $K = Z_t$  households can be simultaneously served within a single resource block. In order to supply all users with individual data, scheduling is necessary, i.e. the  $K_{\text{tot}}$  UTs must be divided into groups of at most  $Z_t$  users. Hence, in addition to spatial multiplexing, a further multiple access scheme like TDMA is necessary to support all users with individual data. Note that, without spatial multiplexing,  $K_{\text{tot}}$  resource blocks

would be necessary whereas the necessary resource blocks reduces to  $K_{\text{tot}}/K$  with spatial multiplexing.

As a major finding of Section II it can be stated that the achievable data rate of a multiuser MIMO SATCOM scenario crucially depends on the location of the involved antennas. Since the locations of the users are arbitrary and do not follow any regular placement, an analytic solution for the optimal placement, like the one that has been derived in (21) for ULA arrangements, cannot be found here. However, the requirement of pairwise orthogonal channel vectors as formulated in (8) still holds.

Assume an optimal setup in the sense of (8), then all  $K$  UTs of a group have orthogonal channel vectors. In this case, ZF precoding does not suffer from any power penalties due to the channel inversion, and can, therefore, achieve the dirty paper coding (DPC) rate region. However, the probability that such a set of UTs exists is zero for a finite  $K_{\text{tot}}$  [48]. Therefore, we aim at combining UTs with channel vectors that are “nearly” or “at most” orthogonal. The orthogonality between the  $i$ -th and the  $j$ -th UT is quantified by means of the scalar product of the channel vectors

$$\cos(\angle(\tilde{\mathbf{h}}_{d,i}, \tilde{\mathbf{h}}_{d,j})) = \left| \tilde{\mathbf{h}}_{d,i}^H \tilde{\mathbf{h}}_{d,j} \right| / (\|\tilde{\mathbf{h}}_{d,i}\| \|\tilde{\mathbf{h}}_{d,j}\|), \quad (35)$$

where  $\angle(\tilde{\mathbf{h}}_{d,i}, \tilde{\mathbf{h}}_{d,j})$  refers to the enclosed angle of the vectors  $\tilde{\mathbf{h}}_{d,i}$  and  $\tilde{\mathbf{h}}_{d,j}$ . The channel vectors are orthogonal if  $\cos(\angle(\tilde{\mathbf{h}}_{d,i}, \tilde{\mathbf{h}}_{d,j})) = 0$ .

In [17] the Multiple Antenna Downlink Orthogonal Clustering (MADOC) scheduling algorithm has first been published, in which (35) is used as a metric to determine the spatial compatibility between two UTs and to build up so-called  $\epsilon$ -orthogonal groups. The main idea is to assemble UTs in a common group only if (35), calculated for all combinations of UTs within a group, does not exceed a certain threshold  $\epsilon$ . The proposed algorithm in [17] is used in this paper to schedule all households into  $N_G$  disjoint groups. In the optimal case, the downlink channel matrix  $\tilde{\mathbf{H}}_d$  is

then composed of perfectly orthogonal row vectors, and each household in each group receives then individual data content without any CCI. While we utilize the MADOC algorithm in this paper to form user groups for unicast transmission over several beams, its metric can similarly be applied to realize a multicast transmission over a single beam. In this case, (35) aims to identify channel vectors that are parallel. For the first time, this algorithm takes advantage of the spatial orthogonality offered by the MIMO channel, and the spatial dimension is exploited as a further degree of freedom.

This is indeed a great advantage of the MIMO technology. In other words, although  $K$  users still occupy the same frequency band and polarization like it would be the case in a broadcast application, their spatial separation is now exploited to distribute individual content to different households. This way, MIMO answers the user's expectations for individual content like VoD and supports the transition from broadcast to unicast transmission in future satellite implementations.

### E. Precoding Design

In our HTS scenario, maximal fairness between the selected users should be ensured by the precoder. In a unicast scenario, every customer indeed expects a minimum assured data rate that is guaranteed by the satellite provider according to the contract model. This is fundamentally different to the broadcast scenario where all users receive the same data and the quality-of-experience solely depends on the individual receiving equipment.

The precoding matrix  $\mathbf{B}$  will be optimized using the common ZF criterion. It is known to offer close-to-optimal performance when the noise contribution is limited, which is the case for feeder links, or for a large number of channel outputs as it is the case in the user links [49]. Here, the following condition must be fulfilled:

$$\tilde{\mathbf{H}}_d \tilde{\mathbf{H}}_u \mathbf{B} = \text{diag} \{ \boldsymbol{\mu} \}, \quad (36)$$

with  $\boldsymbol{\mu} = [\mu_1, \dots, \mu_{Z_t}]^T$ , a vector of non-negative numbers. A max-min fairness optimization problem

can then be formulated as

$$\begin{aligned} & \max_{\boldsymbol{\mu} \geq \mathbf{0}, \mathbf{B}, a_S} \quad \min_k a_S \mu_k \\ & \text{s.t.} \quad \tilde{\mathbf{H}}_d \tilde{\mathbf{H}}_u \mathbf{B} = \text{diag} \{ \boldsymbol{\mu} \} \\ & \quad \text{tr} \{ \mathbf{B}^H \tilde{\mathbf{Q}}_n \mathbf{B} \} \leq P_u, \quad n = 1, 2 \\ & \quad a_S^2 \cdot [\tilde{\mathbf{H}}_u \mathbf{B} \mathbf{B}^H \tilde{\mathbf{H}}_u^H + 2\sigma_{\eta_u}^2 \mathbf{I}_{Z_t}]_{z,z} \leq P_d, \forall z. \end{aligned} \quad (37)$$

The solution of (37) entails  $\boldsymbol{\mu} = \mu \mathbf{1}$  [50]. Moreover, since the noise contribution in the feeder link is limited, the third constraint of (37) can be relaxed by assuming that  $2\sigma_{\eta_u}^2 \ll [\tilde{\mathbf{H}}_u \mathbf{B} \mathbf{B}^H \tilde{\mathbf{H}}_u^H]_{z,z}$ ,  $\forall z$ , and the optimization problem is now expressed as

$$\begin{aligned} & \max_{\mu \geq 0, \mathbf{W}, a_S} \quad a_S \mu \\ & \text{s.t.} \quad \mu^2 \cdot \text{tr} \{ \bar{\mathbf{B}}^H \tilde{\mathbf{Q}}_n \bar{\mathbf{B}} \} \leq P_u, \quad n = 1, 2 \\ & \quad a_S^2 \mu^2 \cdot [\tilde{\mathbf{H}}_u \bar{\mathbf{B}} \bar{\mathbf{B}}^H \tilde{\mathbf{H}}_u^H]_{z,z} \leq P_d, \forall z, \end{aligned} \quad (38)$$

where  $\bar{\mathbf{B}} = \tilde{\mathbf{H}}_u^+ \tilde{\mathbf{H}}_d^+ + \mathbf{P}_\perp \mathbf{W}$  and  $\mathbf{P}_\perp$  is the orthogonal projection into the null space of  $\tilde{\mathbf{H}}_d \tilde{\mathbf{H}}_u$ . Matrix  $\mathbf{W}$  is an arbitrary complex matrix. The reformulation of the optimization problem relies on the fact that a precoding matrix fulfilling the condition of (36) is of the form  $\mathbf{B} = \mu \bar{\mathbf{B}}$  [50]. It corresponds to a generalized inverse of  $\tilde{\mathbf{H}}_d \tilde{\mathbf{H}}_u$ . A solution to (38) is then obtained with

$$\mu = \sqrt{P_u / \max \{ \text{tr} \{ \bar{\mathbf{B}}^H \tilde{\mathbf{Q}}_n \bar{\mathbf{B}} \} \}}, \quad (39)$$

$$a_S = \sqrt{P_d / \mu^2 \cdot \max \{ [\tilde{\mathbf{H}}_u \bar{\mathbf{B}} \bar{\mathbf{B}}^H \tilde{\mathbf{H}}_u^H]_{z,z} \}}, \quad (40)$$

and the matrix  $\bar{\mathbf{B}}$  is determined with the following second-order cone program

$$\min_{\mathbf{W}, t} \quad \text{s.t.} \quad [\tilde{\mathbf{H}}_u \bar{\mathbf{B}} \bar{\mathbf{B}}^H \tilde{\mathbf{H}}_u^H]_{z,z} \leq t. \quad (41)$$

Interestingly, the precoding matrix  $\mathbf{B}$  obtained with (38) leads to the same performance as the precoder  $\mathbf{B} = \mu \mathbf{B}_u \mathbf{B}_d$  where  $\mathbf{B}_u$  and  $\mathbf{B}_d$  are the solutions of a max-min fairness optimization problem for the downlink and the uplink, respectively.<sup>7</sup> The generalized inverse of the product of  $\tilde{\mathbf{H}}_d$  with the square non-singular matrix  $\tilde{\mathbf{H}}_u$  is indeed equal to the product of the inverse of  $\tilde{\mathbf{H}}_u$  and the generalized inverse of  $\tilde{\mathbf{H}}_d$  [51]. Simulation results in Section

<sup>7</sup>Note that, in this case, CSI of  $\tilde{\mathbf{H}}_u$  and  $\tilde{\mathbf{H}}_d$  must be available instead of the entire link from the gateway to the UTs. To obtain  $\tilde{\mathbf{H}}_u$  and  $\tilde{\mathbf{H}}_d$  separately, ad-hoc and different training sequences for the feeder link and the user link are required.



IV will validate the equality of both approaches. A cascade design takes into account the fact that the matrices  $\mathbf{B}_u$  and  $\mathbf{B}_d$  do not need to be updated at the same rate. In a practical system, the matrix  $\tilde{\mathbf{H}}_d$  and, thus, the precoder  $\mathbf{B}_d$  will change at a rate of a few milliseconds. This fast change is not due to the coherence time of the downlink channel but to the user scheduling. Different groups are indeed served in successive time slots. On the other hand, the characteristics of the uplink MIMO channel  $\tilde{\mathbf{H}}_u$  do not evolve so fast, as the same fixed gateway antennas are always used. The only source of random variation in the uplink are the weather impairments. Their coherence time is at least a few hundreds of milliseconds, and the same uplink precoding matrix  $\mathbf{B}_u$  can be used during this time.

### F. Comparison to the State-of-the-Art

For the first time we address both, the application of spatial MIMO in the feeder link and the use of FFR in the user link over a transparent GEO relay. System architectures in the existing literature are limited to either MIMO in the feeder link<sup>8</sup> or MIMO related approaches based on FFR with a multibeam architecture in the downlink (e.g. in [2], [4], [47]).

The second fundamental difference to the current state-of-the-art is that in our approach the signal phase of the LOS part of the channel is exploited. The vast majority of publications do not consider the signal phase of the LOS satellite channel in their models. For example, the authors in [5], [6], [52] assume a uniformly distributed channel phase in the downlink, irrespective of the user's location and the position of the feed on the payload. The authors in [43] state that the phase information in the design of the precoder is neglected. Therefore, the grouping of users as well as the precoder design can only rely on the amplitude information. Simulation results in Section IV will show that, in this case, the achievable rate is limited. A payload with multiple spatially separated antennas, as proposed here, would have no advantage compared to a payload with a single reflector if only the amplitude information is exploited.

While neglecting the phase of the LOS path might be valid as long as a single antenna on the satellite is

<sup>8</sup>To the best of our knowledge, the two paper [20], [32] are the only contributions so far considering the concept of MIMO in the feeder links.

assumed, it becomes inappropriate if multiple antennas are considered. Many satellites currently under procurement offer at least four reflectors mounted as side-deployable antennas at a separation of 6 m to 10 m. These architectures offer the chance to exhibit additional multiplexing gains when resorting to schemes that take the signal phase into account.

### G. Performance Criterion

To assess the performance of the proposed MIMO HTS system the sum achievable rate is used. The sum achievable rate can be obtained by first computing for each user its input-output mutual information. To this end, we define an auxiliary model from (33). Using  $\mathbf{C} = a_S \tilde{\mathbf{H}}_d \tilde{\mathbf{H}}_u \mathbf{B}$ , we can write

$$\begin{aligned} \hat{\mathbf{s}} &= \text{diag}\{\mathbf{C}\} \mathbf{s} + (\mathbf{C} - \text{diag}\{\mathbf{C}\}) \mathbf{s} + a_S \tilde{\mathbf{H}}_d \boldsymbol{\eta}_u + \boldsymbol{\eta}_d \\ &= \text{diag}\{\mathbf{C}\} \mathbf{s} + \bar{\boldsymbol{\eta}}, \end{aligned} \quad (42)$$

where  $\bar{\boldsymbol{\eta}}$  is a vector gathering the contributions of the uplink and downlink noise as well as the inter-stream interference if  $\mathbf{C}$  is non-diagonal. We note that matrix  $\mathbf{C}$  will not be diagonal if  $\tilde{\mathbf{H}}_u$  or  $\tilde{\mathbf{H}}_d$  are rank deficient, i.e. that no zero-forcing is possible.

In practice a satellite link will be designed to avoid such a configuration. In the uplink this is ensured if the gateway antennas are located following the design criteria of (21). In the downlink this is ensured if the users who are jointly considered have nearly orthogonal channel vectors according to (8).

Assuming a circularly-symmetric complex Gaussian distribution for the inter-stream interference, the channel law for the  $k$ -th user in a given resource block is

$$\mathcal{P}(\hat{s}_k | s_k) = \frac{1}{2\pi\sigma_{\bar{\boldsymbol{\eta}},k}^2} \cdot \exp\left\{-\frac{|\hat{s}_k - c_{kk}s_k|^2}{2\pi\sigma_{\bar{\boldsymbol{\eta}},k}^2}\right\} \quad (43)$$

with  $c_{kk}$  the  $k$ -th diagonal element of  $\mathbf{C}$  and  $2\sigma_{\bar{\boldsymbol{\eta}},k}^2$  the variance of the  $k$ -th entry of the vector  $\bar{\boldsymbol{\eta}}$ .

With the knowledge of (43), the input-output mutual information in bit/channel use for the  $k$ -th user is given by

$$\mathcal{I}_k = \mathbb{E}\left\{\log_2\left(\frac{\sum_{s \in \mathcal{A}} \mathcal{P}(\hat{s}_k | s)}{\mathcal{P}(\hat{s}_k | s_k)}\right)\right\}. \quad (44)$$

The application of (44) assumes a maximum-likelihood (ML) symbol detection.

Moreover, we introduce the spectral efficiency

$$C_k = \log_2(1 + \text{CINR}_k), \quad (45)$$

of the  $k$ -th user channel for comparison, where  $\text{CINR}_k = c_{kk}/\sigma_{\eta,k}^2$  denotes the CINR of user  $k$ .

According to the considered input constellation (discrete modulation alphabet or Gaussian distributed input symbols), the achievable rate in bit/s is obtained from the mutual information  $\mathcal{I}_k$  or the spectral efficiency  $C_k$  by normalization with the symbol duration  $T_s$ , i.e.  $\mathcal{R}_k = 1/T_s \cdot \mathcal{I}_k$  or  $\mathcal{R}_k = 1/T_s \cdot C_k$ . The sum achievable rate is then given by

$$\mathcal{R} = \frac{1}{N_G} \sum_{g=1}^{N_G} \sum_{k=1}^{K^g} \mathcal{R}_k^g, \quad (46)$$

where the superscript  $g$  is introduced to take into account the fact that several user groups are considered. Thus,  $K^g$  and  $\mathcal{R}_k^g$  denote the number of users and the achievable rate of user  $k$  in group  $g$ , respectively. Finally, the rate per user beam  $\bar{\mathcal{R}}$  is defined as  $\bar{\mathcal{R}} = \mathcal{R}/Z_t$ .

The sum achievable rate  $\mathcal{R}$  defined in (46) together with the rate per user beam  $\bar{\mathcal{R}}$  allows us to assess the performance of the proposed MIMO HTS system. These two metrics are used in the next section to evaluate the benefit of spatial MIMO in the uplink and the downlink.

#### IV. MIMO HTS SIMULATION RESULTS

The proposed MIMO uplink and downlink architectures will now be evaluated for a satellite positioned at the longitude  $\theta_S = 115^\circ$  W. The feeder uplink operates in the V-band, and the user downlink is in the Ka-band. The gateway array has an orientation  $\delta_E = 0^\circ$ . It is located at latitude  $\phi_E = 38^\circ$  N and longitude  $\theta_E = 98^\circ$  W. Finally, the  $Z_t = 16$  user beams in an SFPB architecture cover the U.S. West Coast where a total of  $K_{\text{tot}} = 4,000$  households have to be served.

We assume a symbol rate of  $1/T_s = 10$  MHz per customer. If the carrier spacing equals  $1.05/T_s$ , up to  $N_c = \lfloor 500 \text{ MHz} \cdot T_s / 1.05 \rfloor = 47$  carriers via FDMA are supported by the 500 MHz downlink beams.

To emphasize the benefits of spatial multiplexing for an HTS system, the uplink and the downlink of the system proposed in Section III will be successively replaced by a state-of-the-art approach. Here, the two following configurations will be investigated in terms of the sum achievable data rate:

- A  $2 \times 2$  MIMO feeder link is compared to a SISO feeder link with single-site diversity, i.e.

TABLE I  
PARAMETERS FOR THE FEEDER LINK EVALUATION

	<i>SISO feeder link</i>	<i>MIMO feeder link</i>
Frequency bands	42.5-43.5 GHz + 47.2-50.2 GHz	
Downlink feeds $Z_t$	16	
Usable bandwidth per downlink beam	250 MHz	500 MHz
Gateway antenna gain	61.4 dBi	
Transmit power per gateway antenna	22 dBW	19 dBW
Satellite $G/T$	26 dB/K	
<i>Downlink configuration</i>		
Architecture	MU-MIMO FFR	
CNR at the center of a beam $\text{CNR}^{\text{bc}}$	10 dB	

one SISO gateway antenna is active while the second SISO gateway antenna is in stand-by.

- A MU-MIMO downlink is compared to a conventional FR4 SISO approach.

In addition to the sum achievable data rate we also assess the vulnerability of the feeder link to rain fading events. As it has already been mentioned in Section II-F, a Q/V-band feeder link may suffer from rain fading events resulting in additional attenuations of several decibel. The simulations will show how MIMO feeder links can take advantage of an additional site diversity gain that directly increases the system availability.

##### A. Feeder Link Performance

The system parameters for the analysis of the feeder link are provided in Table I. Here the objective is to assess the performance of a  $2 \times 2$  MIMO feeder link in terms of the sum achievable data rate. The available bandwidth in the feeder uplink is 4 GHz. Due to the  $2 \times 2$  spatial multiplexing in the MIMO feeder link, a total of 8 GHz usable bandwidth is available in the user downlink.  $Z_t = 16$  downlink feeds should be supported and, thus, the households in each downlink beam can be served with 500 MHz of bandwidth.<sup>9</sup> The SISO feeder link instead can only support a bandwidth of 4 GHz in total, and, therefore, the total bandwidth per downlink beam is set for this benchmark system to 250 MHz. In this case, the number of carriers

<sup>9</sup>Please have in mind that we assume a transparent satellite payload.

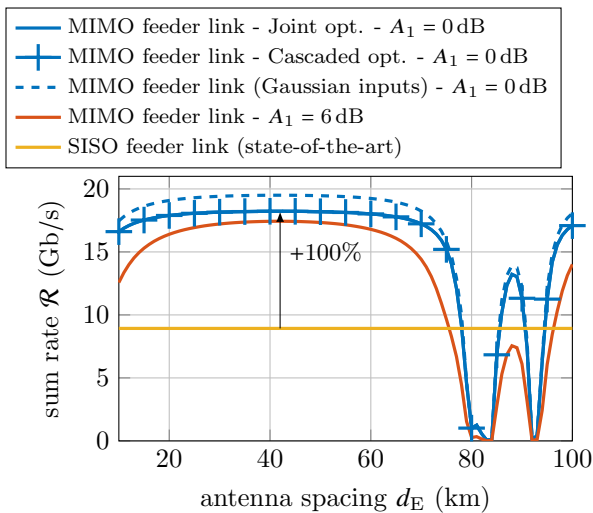


Fig. 8. Sum rate vs. gateway antenna spacing  $d_E$  for two different weather conditions at gateway antenna one while gateway antenna two experience clear sky, i.e.  $A_2 = 0$  dB.

which can be supported via FDMA reduces to  $[250 \text{ MHz} \cdot T_s / 1.05] = 23$ .

In order to still meet coordinated power density limits, the EIRP of the MIMO feeder link must be the same as of the SISO feeder link. Therefore, the transmit power per gateway antenna is 3 dB less in the case of a MIMO gateway antenna. We assume a gateway antenna gain of 61.4 dBi, and, together with a  $G/T$  of 26 dB/K per satellite antenna<sup>10</sup>, the feeder link budget is fully defined. Under clear sky conditions an uplink CNR of 24 dB is achieved.

For the user links a MU-MIMO FFR approach with a CNR of 10 dB at the center of the spot beams is always assumed. It ensures that the differences in terms of sum achievable rate between the SISO and the MIMO feeder links are, in this case, only influenced by the uplink design.

In Fig. 8, the influence of the gateway separation  $d_E$  on the sum achievable rate is shown for two different weather conditions. In one scenario, the first gateway antenna does not experience any rain attenuation, i.e.  $A_1 = 0$  dB, while the other scenario assumes a medium rain attenuation of  $A_1 = 6$  dB. The second gateway antenna benefits in both scenarios from clear-sky conditions, i.e.  $A_2 = 0$  dB. For

<sup>10</sup>The  $G/T$  of 26 dB/K is based on an antenna with diameter of 1.2 m, efficiency of 55% at 48 GHz and a system temperature of 500 K [53]. Since the center of coverage of both satellite antennas is at the center of the gateway array, the offaxis angle from point of boresight is only  $0.017^\circ$ . The resulting depointing loss is only 0.02 dB. This value is too small to make a difference in the simulation results and has, therefore, been neglected.

the sake of illustration, results obtained with a joint optimization and a cascaded optimization of the precoding matrix are shown in the case  $A_1 = 0$  dB. The goal is to confirm that both optimizations lead actually to the same precoder. This property has been emphasized in Section III-E. Moreover, for comparison purposes the sum achievable rate based on the spectral efficiency according to (45) is provided (dashed blue curve). Finally, the achievable rate of a state-of-the-art SISO feeder link is also displayed. In this configuration, the second gateway antenna is the only active ground station.

The sum achievable rate is maximized for a separation of around 40 km but a large range of  $\pm 15$  km relative to the optimal position can be accepted without entailing serious performance degradations. The improved sum data rate of the MIMO solution is the result of spatial multiplexing in the feeder uplink. Although 4 GHz of bandwidth is allocated in the feeder uplink, 8 GHz of user link bandwidth instead of 4 GHz for the state-of-the-art can be used to serve the 4,000 households in the downlink. It can be noted that the minima for values of  $d_E$  near 80 km and 90 km are due to the presence of close-to-singular MIMO channel matrices in the bands 47.2-50.2 GHz and 42.5-43.5 GHz, respectively. However, distances of more than 80 km do not belong to the region of interest for a practical system design.

The curves show also that an additional atmospheric attenuation does not severely degrade the data rate performance of the MIMO feeder link. Even for a rain attenuation of  $A_1 = 6$  dB at gateway antenna one, the MIMO feeder link still outperforms the state-of-the-art SISO approach even in clear-sky. One reason for this small degradation is clearly the 14 dB higher uplink CNR compared to the downlink CNR (24 dB in the uplink vs. 10 dB in the downlink). However, an additional attenuation of 6 dB at one antenna does, nevertheless, not result in a 6 dB lower CNR in one of the two equivalent SISO sub-channels. In fact, since in an optimal MIMO channel both gateway antennas contribute equally to the receive CNR, an attenuation of 6 dB at one gateway antenna results only in a 3 dB lower CNR per receive antenna. Apart from the multiplexing gain, the additional spatial domain usage of the MIMO approach inherently provides a higher robustness against weather effects [54]. In other words: The results clearly suggest to avoid so-called “cold redundancy” w.r.t. gateway antennas, i.e. it is

TABLE II  
PARAMETERS FOR THE USER LINK EVALUATION

	<i>SISO FR4</i>	<i>MU-MIMO FFR</i>
Downlink feeds $Z_t$		16
Bandwidth per beam	125 MHz	500 MHz
Downlink EIRP per beam $P_d$	51 dBW to 65 dBW	
User terminal $G/T$	16.9 dB/K	
Resulting CNR at beam center CNR <sup>bc</sup>	6 dB to 20 dB	0 dB to 14 dB
<i>Uplink configuration</i>		
Architecture	MIMO feeder link with $d_E = 40$ km	
Frequency bands	42.5-43.5 GHz	42.5 – 43.5 GHz 47.2 – 50.2 GHz

better to switch all available antennas on and operate them as a MIMO feeder link instead of preserving antennas for outage redundancy only.

The results presented in this section illustrate the potential of the spatial MIMO concept for the feeder links of HTS systems. The possibility to distribute spatially multiplexed signals containing individual content for multiple users perfectly supports the resort of the conventional television (TV) broadcast scenario to unicast transmission. Please note again that the goal of this simulation example was to illustrate how spatial multiplexing can generally be realized in a single feeder link.

As already mentioned earlier, several tens of spatially separated feeder links are necessary in practice [36], and, in this case, the advantage of the MIMO approach lies in the reduction of the interference between neighboring feeder links. Less geographically separated MIMO feeder links than SISO feeder links are required to provide a given amount of data to serve all households with different content in a practical HTS. Therefore, if the feeder links have to be deployed in a certain country or continent, interference can be more easily avoided by guaranteeing a larger angular separation between the beams [32]. This is especially advantageous in terms of system availability as better link budgets reduce the probability of experiencing an outage when rain events affect the link quality [20].

### B. User Link Performance

The second simulation aims to investigate the data rate performance of the proposed multiuser MIMO downlink. The objective is to show the advantage of

having multiple spatially separated antennas on the satellite in combination with full frequency reuse among the user beams. The result is compared to a contemporary SISO scheme that is based on a single-reflector with four color frequency reuse. To highlight the importance of spatially separated antennas to benefit from a MIMO gain, the multiple-reflector approach is also compared to a MIMO downlink based on a single-antenna with multiple beams and FFR.

The system parameters for this simulation are provided in Table II. As already introduced in Section III-A, four reflectors form a circular array with a diameter of 3 m, and four feeds illuminate each reflector. Each reflector has a diameter of 2.6 m. The feed and reflector geometry is based on a satellite that is currently in orbit [55]. In our simulation scenario, the service zone of the  $Z_t = 16$  spot beams is over North America, and we assume 250 independent and fixed single-antenna receivers per beam. The location of an individual user is randomly chosen; all users are uniformly distributed over the entire service zone. Hence, in total  $K_{\text{tot}} = 16 \cdot 250 = 4,000$  households need to be served with data.<sup>11</sup>

The user scheduling algorithm from [17] is now applied to determine those households that form a common group. The total number of groups and the number of households in each group actually depend on several parameters. Among others, we observe a dependence on the location of the users, the threshold  $\epsilon$ , the signal-to-noise ratio and the total number of households that have to be scheduled [17]. In this simulation example, for instance, we obtained the set of  $N_G = 311$  user groups. Thus, in total  $N_G = 311$  MIMO downlink channel matrices  $\mathbf{H}_d \in \mathbb{C}^{K \times Z_t}$  are computed. For each UT we assume similar receiving equipment having a  $G/T$  of 16.9 dB.

In order to show the benefit of spatial MIMO for different signal-to-noise ratios, various downlink EIRP values  $P_d$  are simulated in each beam ranging from 51 dBW to 65 dBW. Please note again that, in the case of MIMO,  $P_d$  constitutes the maximum power in at least one of the MIMO beams while the power in the remaining beams can actually be equal to or lower than  $P_d$ . This is the result of the

<sup>11</sup>This simulation scenario and the parameter setup have partly been published in [17]. For an illustration of the antenna geometry on the satellite we kindly refer to Fig. 1 in [17].

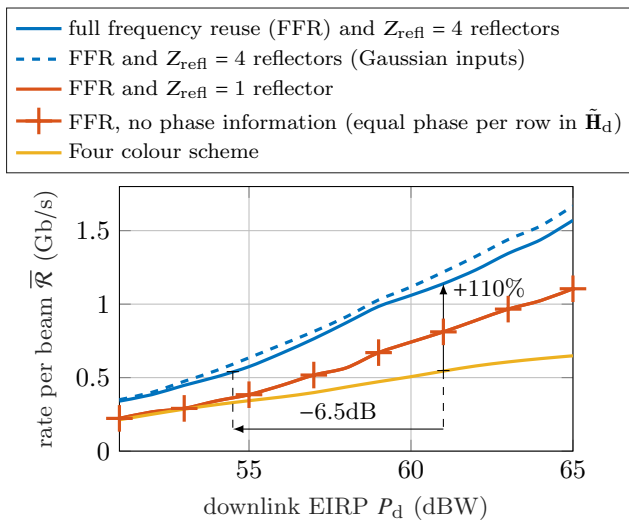


Fig. 9. Achievable rate per beam as a function of the downlink EIRP using a MIMO feeder link with  $d_E = 40$  km and clear-sky conditions at both gateway stations.

power constraint as defined in (32). In the SISO case instead, each beam provides the maximum downlink EIRP  $P_d$ . Thus, the sum power over all beams of the SISO downlink is always higher or at most equals the sum power of the MIMO downlink. This ensures a fair comparison between MIMO and SISO.

Moreover, in the FFR scheme the entire bandwidth of 500 MHz within the range of 19.7 GHz to 20.2 GHz is available in each beam. In the case of the four-color scheme instead, only 125 MHz per beam can be used. To ensure a fair comparison, the transmit power per beam is equal for both, the FFR and the FR4 scheme. As a consequence, the resulting receive CNR is even 6 dB higher for the FR4 scheme than for the FFR scheme.

Since the focus is now on the performance of the multiuser downlink, the feeder uplink configuration is identical for all considered cases. In particular, a  $2 \times 2$  MIMO feeder link in the V-band is assumed, and the gateway antennas have a spacing of  $d_E = 40$  km. Please note that, to support the aggregated bandwidth in the user link, the occupied bandwidth in the feeder link is adjusted accordingly. While for the FR4 scheme 1 GHz of bandwidth is sufficient, 4 GHz of bandwidth is necessary to support the FFR approach. A constant uplink receive CNR of 24 dB is achieved in all cases.

Fig. 9 provides the simulation results of the sum achievable rate per user beam as a function of the downlink EIRP  $P_d$ . The blue curve corresponds to the proposed MU-MIMO FFR strategy with  $Z_{\text{reff}} =$

4 reflectors. Moreover, the channel capacity based on (45) is shown again (blue dashed curve). The yellow curve shows the result of the state-of-the-art FR4 approach with 125 MHz per user beam. As mentioned earlier, the result of a MIMO downlink with a single-reflector that generates all the user beams is also provided (red curve). Finally, the simulation results for the case that no phase information in the downlink channel is considered are also shown (red crosses). As mentioned in Section III-F, this curve represents the channel model assumptions from [5], [6], [52], in which no LOS channel phase information can be exploited to form user groups or derive the precoder. The absence of LOS channel phase information can be manifold, for instance due to the use of a single-reflector architecture in the satellite or due to very narrow satellite and ground antenna spacings. This explains why the LOS phase information might not be included in the models of some state-of-the-art works.

The MU-MIMO downlink with four separated antennas offers the highest sum achievable data rate in all considered cases. To give an example: Comparing the blue and the yellow curves at  $P_d = 61$  dBW, the MU-MIMO downlink achieves 1.2 Gb/s per beam compared to 0.55 Gb/s only for the SISO FR4 approach. This constitutes an increase of 110%. The satellite operator has now various options how this gain can be exploited:

- 1) Provide simply higher data rates to the households,
- 2) Keep the sum data rate constant and reduce the necessary downlink EIRP instead, or
- 3) exploit the gain as an additional link margin to increase the availability of the downlink.

For example, keeping the sum achievable data rate constant would allow for a reduction of the required downlink EIRP by 6.6 dB. This reduction could be transferred into a lower payload weight and power budget and, finally, cost reduction. As an alternative, the interference potential in terms of downlink adjacent satellite interference can be reduced.

Moreover, the MIMO downlink with four spatially separated reflectors indeed outperforms the multibeam MIMO approach based on a single-reflector. The reason is simply that the spacing of the feed elements is much smaller (in the centimeter-range) for the single-reflector approach compared to the four separated reflectors (in the meter-range). As a consequence, the spacing between two house-

holds who are part of the same group needs to be much larger<sup>12</sup>, e.g. more than 1,000 km compared to around 50 km. Since, in addition, the 3 dB-contour of one beam footprint is  $\approx 500$  km, the signal energy that can be received from neighboring MIMO beams is comparably low. In other words, the interference from neighboring MIMO beams, which we are seeking to exploit as information bearing signal, is very low due to this large separation of two households who are jointly served with data. Low signal interference results in a MIMO downlink channel matrix with small values, and the multiplexing gain is ultimately limited.

To sum up, the simulation results have shown the data rate advantage of spatial multiplexing in both, the uplink and the downlink. Through multiplexing of different data streams, multiple users can be served simultaneously over the same channel. The gain of our system proposal relies on the spatial separation of the MIMO antennas.

## V. CONCLUSION

In this work the theoretical basics of the MIMO line-of-sight concept for fixed satellite services have been presented. It has been shown that the phase of the LOS signal is the key parameter to understand the possible gains of a MIMO SATCOM system. By appropriately paying attention to the signal phase, the optimal location of the MIMO antennas on earth and in orbit have been derived.

As a promising application example, the design of future HTS systems has been addressed. Our system proposal considered both, the use of spatial multiplexing in the feeder uplink and in the multiuser downlink. While simultaneously resorting from the conventional four color frequency reuse to the full frequency reuse scheme in the downlink, the resulting inter-beam interference can now be exploited as a useful signal energy that further increases the throughput. Based on user scheduling and MU-MIMO precoding in the gateway, single-antenna users are now able to receive individual data streams over the same channel. Simulation results have shown tremendous performance gains in terms of the sum achievable data rate in comparison to

the state-of-the-art. The MIMO technology is a key enabler to boost the competitiveness of satellite communications in 5G networks.

## REFERENCES

- [1] S. K. Sharma, S. Chatzinotas, and P.-D. Arapoglou, *Satellite Communications in the 5G Era*. Institution of Engineering and Technology, 2018.
- [2] M. A. Vazquez, A. Perez-Neira, D. Christopoulos, S. Chatzinotas, B. Ottersten, P.-D. Arapoglou, A. Ginesi, and G. Tarocco, "Precoding in Multibeam Satellite Communications: Present and Future Challenges," *IEEE Wirel. Commun.*, vol. 23, no. 6, pp. 88–95, dec 2016.
- [3] D. Christopoulos, S. Chatzinotas, G. Zheng, J. Grotz, and B. Ottersten, "Linear and nonlinear techniques for multibeam joint processing in satellite communications," *EURASIP Journal on Wireless Communications and Networking*, vol. 2012, no. 1, p. 162, 2012.
- [4] J. Arnau, B. Devillers, C. Mosquera, and A. Pérez-Neira, "Performance study of multiuser interference mitigation schemes for hybrid broadband multibeam satellite architectures," *EURASIP Journal on Wireless Communications and Networking*, vol. 2012, no. 1, p. 132, apr 2012.
- [5] D. Christopoulos, S. Chatzinotas, and B. Ottersten, "Multicast Multigroup Precoding and User Scheduling for Frame-Based Satellite Communications," *IEEE Trans. Wirel. Commun.*, vol. 14, no. 9, pp. 4695–4707, sep 2015.
- [6] V. Joroughi, M. A. Vazquez, and A. I. Perez-Neira, "Generalized Multicast Multibeam Precoding for Satellite Communications," *IEEE Trans. Wirel. Commun.*, vol. 16, no. 2, pp. 952–966, feb 2017.
- [7] European Telecommunications Standards Institute, "Digital Video Broadcasting (DVB); Second generation framing structure, channel coding and modulation system for Broadcasting, Interactive Services, News Gathering and other broadband satellite applications; Part 2: DVB-S2 Extension (DVB-S2X)," 2014.
- [8] T. D. Cola, D. Tarchi, and A. Vanelli-Coralli, "Future trends in broadband satellite communications: information centric networks and enabling technologies," *Int. J. Satell. Commun. Netw.*, vol. 33, no. 5, pp. 473–490, sep 2015.
- [9] A. Kyrgiazos, B. Evans, P. Thompson, P. T. Mathiopoulos, and S. Papaharalabos, "A terabit/second satellite system for European broadband access: a feasibility study," *Int. J. Satell. Commun. Netw.*, vol. 32, no. 2, pp. 63–92, mar 2014.
- [10] G. A. Siles, J. M. Riera, and P. Garcia-del Pino, "Atmospheric Attenuation in Wireless Communication Systems at Millimeter and THz Frequencies [Wireless Corner]," *IEEE Antennas Propag. Mag.*, vol. 57, no. 1, pp. 48–61, feb 2015.
- [11] A. Gharanjik, B. Shankar, P.-D. Arapoglou, and B. Ottersten, "Multiple Gateway Transmit Diversity in Q/V Band Feeder Links," *IEEE Trans. Commun.*, vol. 63, no. 3, pp. 916–926, mar 2015.
- [12] P. Driessen and G. Foschini, "On the capacity formula for multiple input-multiple output wireless channels: a geometric interpretation," *IEEE Trans. Commun.*, vol. 47, no. 2, pp. 173–176, feb 1999.
- [13] R. T. Schwarz, A. Knopp, D. Ogermann, C. A. Hofmann, and B. Lankl, "Optimum-capacity MIMO satellite link for fixed and mobile services," in *2008 Int. ITG Work. Smart Antennas, WSA 2008*, feb 2008, pp. 209–216.

<sup>12</sup>Please note again the linear relation  $d_S d_E \propto r \lambda_c$  between the antenna spacing as a function of the wavelength  $\lambda_c$  and the UT-satellite distance  $r$ , which has been introduced in Section II. As a result, the smaller the spacing in orbit the larger the spacing on earth has to be.

- [14] K.-U. Storek, C. A. Hofmann, and A. Knopp, "Measurements of phase fluctuations for reliable MIMO space communications," in *2015 IEEE Asia Pacific Conf. Wirel. Mob.*, no. 1. IEEE, aug 2015, pp. 157–162.
- [15] C. Hofmann, K.-U. Storek, R. T. Schwarz, and A. Knopp, "Spatial MIMO over satellite: A proof of concept," in *2016 IEEE Int. Conf. Commun.* Kuala Lumpur, Malaysia: IEEE, may 2016, pp. 1–6.
- [16] C. A. Hofmann, R. T. Schwarz, and A. Knopp, "Multisatellite UHF MIMO Channel Measurements," *IEEE Antennas Wirel. Propag. Lett.*, vol. 16, pp. 2481–2484, 2017.
- [17] K. U. Storek and A. Knopp, "Fair User Grouping for Multibeam Satellites with MU-MIMO Precoding," in *GLOBECOM 2017 - 2017 IEEE Global Communications Conference*, Dec 2017, pp. 1–7.
- [18] G. Giambene, S. Kota, and P. Pillai, "Satellite-5G Integration: A Network Perspective," *IEEE Netw.*, vol. 32, no. 5, pp. 25–31, sep 2018.
- [19] G. Maral and M. Bousquet, *Satellite Communications Systems: Systems, Techniques and Technology*, 5th ed. John Wiley & Sons Ltd., 2009.
- [20] T. Delamotte and A. Knopp, "Outage Analysis of a MIMO-Based Smart Gateway Architecture," in *2018 IEEE Int. Conf. Commun.*, may 2018, pp. 1–6.
- [21] International Telecommunication Union, "Radiation diagrams for use as design objectives for antennas of earth stations operating with geostationary satellites," 2003.
- [22] J.-S. Jiang and M. Ingram, "Spherical-wave model for short-range MIMO," *IEEE Trans. Commun.*, vol. 53, no. 9, pp. 1534–1541, sep 2005.
- [23] E. Telatar, "Capacity of Multi-antenna Gaussian Channels," *Eur. Trans. Telecommun.*, vol. 10, no. 6, pp. 585–595, nov 1999.
- [24] I. Sarris and A. Nix, "Design and performance assessment of maximum capacity MIMO architectures in line-of-sight," *IEE Proc. - Commun.*, vol. 153, no. 4, p. 482, aug 2006.
- [25] E. M. Soop, *Handbook of Geostationary Orbits*, 1994th ed., J. R. Wertz, Ed. Kluwer Academic Publishers, 1994.
- [26] B. Ramamurthy, W. G. Cowley, and G. Bolding, "MIMO Applicability to UHF SATCOM," in *IEEE Glob. Telecommun. Conf. (GLOBECOM 2016)*, 2016, pp. 1–7.
- [27] J. E. Allnutt, *Satellite-to-ground radiowave propagation*, 2nd ed., ser. Electromagnetic Waves Series 54. The Institution of Engineering and Technology, 2011.
- [28] R. T. Schwarz, A. Knopp, and B. Lankl, "The channel capacity of MIMO satellite links in a fading environment: A probabilistic analysis," in *IWSSC'09 - 2009 Int. Work. Satell. Sp. Commun. - Conf. Proc.*, sep 2009, pp. 78–82.
- [29] P. Horvath and I. Frigyes, "SAT02-6: Application of the 3D Polarization Concept in Satellite MIMO Systems," in *IEEE Globecom 2006*. IEEE, nov 2006, pp. 1–5.
- [30] R. T. Schwarz, A. Knopp, and B. Lankl, "Performance of an SC-FDE SATCOM system in block-time-invariant orthogonal MIMO channels," *GLOBECOM - IEEE Glob. Telecommun. Conf.*, pp. 1–6, dec 2011.
- [31] X. Zhang, L. Chen, J. Qiu, and J. Abdoli, "On the Waveform for 5G," *IEEE Commun. Mag.*, vol. 54, no. 11, pp. 74–80, nov 2016.
- [32] T. Delamotte, R. T. Schwarz, K.-U. Storek, and A. Knopp, "MIMO Feeder Links for High Throughput Satellites," in *WSA 2018; 22nd Int. ITG Work. Smart Antennas*. VDE, 2018, pp. 1–8.
- [33] K. Y. Lau, G. F. Lutes, and R. L. Tjoelker, "Ultra-Stable RF-Over-Fiber Transport in NASA Antennas, Phased Arrays and Radars," *J. Light. Technol.*, vol. 32, no. 20, pp. 3440–3451, oct 2014.
- [34] P. Angeletti, R. D. Gaudenzi, M. Lisi, I. Introduction, S. Division, and C. Scientist, "From 'Bent Pipes' to 'Software Defined Payloads': Evolution and Trends of Satellite Communications Systems," *System*, no. June, pp. 10 – 12, 2008.
- [35] V. Sulli, D. Giancristofaro, F. Santucci, and M. Faccio, "Computing the hardware complexity of digital transparent satellite processors on the basis of performance requirements," in *2017 IEEE Int. Conf. Commun.* IEEE, may 2017, pp. 1–7.
- [36] O. Vidal, G. Verelst, J. Lacan, E. Albery, J. Radzik, and M. Bousquet, "Next generation High Throughput Satellite system," in *2012 IEEE First AESS Eur. Conf. Satell. Telecommun.* IEEE, oct 2012, pp. 1–7.
- [37] V. Icolari, S. Cioni, P.-d. Arapoglou, A. Ginesi, and A. Vanelli-coralli, "Flexible Precoding for Mobile Satellite System Hot Spots," in *2017 IEEE Int. Conf. Commun.*, 2017.
- [38] C. Qian, S. Zhang, and W. Zhou, "Traffic-based dynamic beam coverage adjustment in satellite mobile communication," in *2014 Sixth Int. Conf. Wirel. Commun. Signal Process.* IEEE, oct 2014, pp. 1–6.
- [39] A. Gharanjik, B. S. M. R. Rao, P.-D. Arapoglou, and B. Ottersten, "Gateway Switching in Q/V Band Satellite Feeder Links," *IEEE Commun. Lett.*, vol. 17, no. 7, pp. 1384–1387, jul 2013.
- [40] A. Kyrgiazos, B. G. Evans, and P. Thompson, "On the Gateway Diversity for High Throughput Broadband Satellite Systems," *IEEE Trans. Wirel. Commun.*, vol. 13, no. 10, pp. 5411–5426, oct 2014.
- [41] N. Jeannin, L. Castanet, J. Radzik, M. Bousquet, B. Evans, and P. Thompson, "Smart gateways for terabit/s satellite," *Int. J. Satell. Commun. Netw.*, vol. 32, no. 2, pp. 93–106, mar 2014.
- [42] C. Caini, G. Corazza, G. Falciasecca, M. Ruggieri, and F. Vatalaro, "A spectrum- and power-efficient EHF mobile satellite system to be integrated with terrestrial cellular systems," *IEEE J. Sel. Areas Commun.*, vol. 10, no. 8, pp. 1315–1325, 1992.
- [43] A. Guidotti, A. Vanelli-Coralli, G. Taricco, and G. Montorsi, "User Clustering for Multicast Precoding in Multi-Beam Satellite Systems," *arXiv Prepr. arXiv1706.09482*, pp. 1–30, jun 2017.
- [44] S. D. Addio and P. Angeletti, "A Survey of Calibration Methods for Satellite Payloads Based on Active Front-Ends," in *32nd ESA Antenna Workshop on Antennas for Space Applications*, Oct 2010, pp. 1–4.
- [45] N. Benvenuto and G. Cherubini, *Algorithms for Communications Systems and their Applications*, 4th ed. John Wiley & Sons, 2002.
- [46] D. Christopoulos, S. Chatzinotas, and B. Ottersten, "Weighted Fair Multicast Multigroup Beamforming Under Per-antenna Power Constraints," *IEEE Trans. Signal Process.*, vol. 62, no. 19, pp. 5132–5142, oct 2014.
- [47] W. Wang, A. Liu, Q. Zhang, L. You, X. Gao, and G. Zheng, "Robust Multigroup Multicast Transmission for Frame-Based Multi-Beam Satellite Systems," *IEEE Access*, vol. 6, pp. 46 074–46 083, 2018.
- [48] C. Swannack, E. Uysal-Biyikoglu, and G. Wornell, "Low complexity multiuser scheduling for maximizing throughput in the MIMO broadcast channel," in *Proc. Allert. Conf. Commun. Control Comput.*, 2004.
- [49] G. Caire and S. Shamai, "On the achievable throughput of a multiantenna Gaussian broadcast channel," *IEEE Trans. Inf. Theory*, vol. 49, no. 7, pp. 1691–1706, jul 2003.
- [50] A. Wiesel, Y. Eldar, and S. Shamai, "Zero-Forcing Precoding

and Generalized Inverses,” *IEEE Trans. Signal Process.*, vol. 56, no. 9, pp. 4409–4418, sep 2008.

- [51] H. Lütkepohl, *Handbook of Matrices*. John Wiley & Sons, 1996.
- [52] M. A. Diaz, N. Courville, C. Mosquera, G. Liva, and G. E. Corazza, “Non-Linear Interference Mitigation for Broadband Multimedia Satellite Systems,” in *2007 Int. Work. Satell. Sp. Commun.* IEEE, sep 2007, pp. 61–65.
- [53] P. Thompson, B. Evans, M. Bousquet, and L. Castenet, “Concepts and Technologies for a Terabit / s Satellite Supporting future broadband services via satellite,” in *Third Int. Conf. Adv. Satell. Sp. Commun.*, 2011, pp. 12–19.
- [54] A. Knopp, R. T. Schwarz, and B. Lankl, “On the capacity degradation in broadband MIMO satellite downlinks with atmospheric impairments,” *IEEE Int. Conf. Commun.*, pp. 1–6, may 2010.
- [55] H. Fenech, A. Tomatis, S. Amos, V. Soumpholphakdy, and J. L. Serrano Merino, “Eutelsat HTS systems,” *Int. J. Satell. Commun. Netw.*, vol. 34, no. 4, pp. 503–521, jul 2016.



systems and software

**Kai-Uwe Storek** (M’15) was born in Eilenburg, Germany, in 1986. He received the Dipl.-Ing. degree in information systems engineering from the Technische Universität Dresden (TUD), in 2013. Currently he is a research associate at the Bundeswehr University Munich, Germany, working towards the Ph.D. degree. His current research interests include MIMO signal processing, scheduling for multiuser defined radios.



**Robert Schwarz** (M’08) received the Dipl.-Ing. degree in electrical engineering and information technology from the Bundeswehr University Munich, Germany, in 2006.

From 2006 to 2012, he was with the Federal Office of the Bundeswehr for Information Management and Information Technology, where he was involved in the German program for satellite communications of the Bundeswehr (SATCOMBw). Since 2012, he has been a Research Fellow with the Bundeswehr University Munich, Germany. His research interests include digital signal processing, waveform design, and MIMO for satellite and non-terrestrial networks.

Mr. Schwarz is a member in the German engineers’ association VDE/ITG.



**Thomas Delamotte** (M’16) was born in Reims, France, 1986. He received the master’s degree in telecommunications and network engineering from the National Polytechnic Institute of Toulouse, France, in 2009.

He is currently working towards the Ph.D. degree in electrical engineering from the Bundeswehr University Munich, Germany. Since 2010, he is working as a research fellow in the Department of Electrical Engineering and Information Technology, Bundeswehr University Munich. He leads the research group “Digital Satellite Payloads & Satellite Monitoring” and is implied in several projects funded by the German Aerospace Center (DLR). His research interests include the application of advanced signal processing techniques and waveform designs for next-generation satellite systems.



**Andreas Knopp** (M’04-SM’17) earned his Ph.D. degree (with distinction) in radio communications from the Bundeswehr University Munich in 2008.

Since 2014 he has been a Full Professor of Signal Processing, coordinating in addition Germany’s largest SpaceCom laboratory and experimental satellite ground station, the Munich Center for Space Communications.

Prior to taking up the faculty position, he gained expertise as a communications engineer and satellite program manager. His current interests include satellite network integration and waveform design for 5G, digital satellite payloads, secure / antijam communications, and low power mTC. He is an entrepreneur and co-founder of two start-up companies implementing his research.

Prof. Knopp is an advisor to the German MoD, a member of the expert group on radio systems in the German engineers’ association VDE/ITG, and a member of AFCEA.